Double-Gated Dielectric Modulated Field Effect Transistors and their Modeling as Biosensors, a Literature Review and design built in the Sentaurus Software Environment

---

THESIS

Submitted in Partial Fulfillment of
the requirements for
the degree of

MASTER OF SCIENCE
(Electrical Engineering)
at the
NEW YORK UNIVERSITY
TANDON SCHOOL OF ENGINEERING

by

Justin Collett

September 2023

Double-Gated Dielectric Modulated Field Effect Transistors and their Modeling as Biosensors, a Literature Review and design built in the Sentaurus Software Environment

---

THESIS

Submitted in Partial Fulfillment of
the requirements for
the degree of

MASTER OF SCIENCE (Electrical Engineering)
at the
NEW YORK UNIVERSITY TANDON SCHOOL OF ENGINEERING

by

Justin Collett

September 2023

Approved:

Davood Shahrjerdi

Advisor Signature

05/09/2023

Date

Ivan Selesnick

Department Chair Signature

June 13, 2023

Date

University ID: N14762199
Net ID: jjc9582

Approved by the Guidance Committee:

Major: Electrical Engineering

Davood Shahrjerdi

Prof. Davood Shahrjerdi
Associate Professor
NYU Tandon School of Engineering
6/8/2023
Date

VTsifri

Prof. Vladimir Tsifrinovich
Industry Professor
NYU Tandon School of Engineering
6/8/2023
Date

Microfilm or other copies of this thesis are obtainable from

UMI Dissertation Publishing

ProQuest CSA

789 E. Eisenhower Parkway

P.O. Box 1346

Ann Arbor, MI 48106-1346

VITA

Justin Collett was born in Newport Beach, California in December 1994. He earned his Bachelors degree in Bioengineering from the University of California, Santa Cruz, with a concentration in Bioelectronics. His senior design project was an EEG prosthetic arm, actuating in accordance to elevated signal above a noise floor detected from an EEG headset. He began his graduate studies at the New York University's Tandon school of Engineering in the semester of Fall 2021, pursuing a Master's degree in Electrical Engineering. The focus of this work, his Master's Thesis, is on the DG-DMFET device structure and its biosensing applications, as well as modeling the design in the Sentaurus software environment. His prior work experience, before beginning his Master's program, is within power engineering, modeling power plants and assessing that NERC standards are met for protection. Now, his current research interests are in Nanotechnology, in which his Thesis work has been advised by Professor Davood Shahrjerdi.

Acknowledgements

I would like to express my appreciation to my academic advisor, Dr. Davood Shahrjerdi, who has provided valuable insights and helped me develop a greater affinity towards research and the design process of nanodevice structures in software modeling environments for intended applications such as bio-sensing.

I would also like to extend my appreciation towards the NYU Tandon IT staff, as well as the general board who manages the Electrical Engineering department, as a lot of hard work is put into configuring the program, including the tools and software used in the construction of this research thesis.

NYU's IT department was instrumental in setting up the server credentials and login credentials to access the Sentaurus software and to work ideally on the research design.

As a final demonstration of my appreciation, I would like to thank the researchers and members who contributed to this subject generally, and I am especially grateful to those who I have used as sources in the literature review segment of this Thesis and whose names are included in the bibliography section.

Dedication

I am grateful to my family and friends who have supported me throughout my academic and other personal endeavors.

ABSTRACT

Double-Gated Dielectric Modulated Field Effect Transistors and their Modeling as Biosensors, a Literature Review and design built in the Sentaurus Software Environment

by

Justin Collett

Advisor: Prof. Davood Shahrjerdi, Ph.D.

Submitted in Partial Fulfillment of the Requirements for the Degree of Master of Science (Electrical Engineering)

September 2023

This thesis will discuss and detail a conceptualized design, showcasing the design strategies, trade-offs, advantages, and future developments, as well as describing the physics involved and engineering developments. An examination of the relevant literature is available, as it relates to the developments within the field, providing insights into design choice advantages via the respective studies' comparative analyses and modelings. The general theory and practical results via simulation are shown within this literature review, and the primary chapter relates to the examined literature. The latter chapter will provide expected results and behavior, where the phenomena is detailed in a greater discussion.

Table of Contents

	Page #
Introduction:	
Guidance Committee page	ii
Dissertation Publication page	iii
Vita	iv
Acknowledgements	v
Dedication	vi
Abstract	vii
List of Figures	ix
List of Tables	xi
Body:	
Chapter 1: DG-DMFET designed in Sentaurus	1
Chapter 2: Literature Review	12
References/Bibliography of Literature Review Sources	66

List of Figures

	Page #
Chapter 1:	
Figure 1.1	3
Figure 1.2	4
Figure 1.3	5
Figure 1.4	5
Figure 1.5	6
Figure 1.6	6
Figure 1.7	9
Figure 1.8	10
Chapter 2:	
Figure 2.1.1	14
Figure 2.1.2	14
Figure 2.1.3	15
Figure 2.1.4	16
Figure 2.1.5	18
Figure 2.1.6	18
Figure 2.1.7	19
Figure 2.1.8	20
Figure 2.1.9	21
Figure 2.1.10	22
Figure 2.1.11	23
Figure 2.2.1	24
Figure 2.2.2	24
Figure 2.2.3	25
Figure 2.2.4	25
Figure 2.2.5	26
Figure 2.2.6	27
Figure 2.2.7	27
Figure 2.2.8	27
Figure 2.2.9	28

Figure 2.3.1 29
Figure 2.3.2 30
Figure 2.3.3 30
Figure 2.3.4 31
Figure 2.3.5 32
Figure 2.3.6 33
Figure 2.4.1 34
Figure 2.4.2 35
Figure 2.4.3 35
Figure 2.4.4 36
Figure 2.4.5 37
Figure 2.4.6 38
Figure 2.4.7 39
Figure 2.4.8 39
Figure 2.5.1 41
Figure 2.5.2 42
Figure 2.5.3 43
Figure 2.5.4 43
Figure 2.5.5 44
Figure 2.6.1 45
Figure 2.6.2 46
Figure 2.6.3 47
Figure 2.6.4 48
Figure 2.6.5 49
Figure 2.6.6 50
Figure 2.6.7 51
Figure 2.7.1 53
Figure 2.7.2 55
Figure 2.7.3 56
Figure 2.7.4 57
Figure 2.7.5 57
Figure 2.8.1 58
Figure 2.8.2 60
Figure 2.8.3 62
Figure 2.8.4 63

List of Tables

	Page #
Table 2.1.1	17
Table 2.1.2	23
Table 2.7.1	54

Double-Gated Dielectric Modulated Field Effect Transistors and their Modeling as Biosensors, a Literature Review and design built in the Sentaurus Software Environment

Chapter 1 –DG-DMFET designed in Sentaurus

This chapter's intent is to discuss the design proposal, constructed in the Synopsys Sentaurus environment, and to discuss the underlying physics, expected design advantages, and subsequent work which would follow to improve the design's performance, obtain further characterizations and modeling. To preface, the following work was completed to the point of having fully compiled designs of double-gated dielectric modulated field effect transistors with and without the nanogap implementations configured. However, similar to some other built-in designs, the analytical modeling stage involved compilation without outputted graphical data or raw data. Various cmd files were programmed to try to generate graphical data or simulation plots via the inspect and svisual tools, as examples, however, the files were not able to be generated and visible in the inspect or svisual tools, similar to other designs. Various research works, which use different TCAD for their analytical modelings, will be referred to, in the following chapter, as expectations of advantageous design decisions, fairly similar expectations of transfer curve characteristics, sensitivity measurements, and indications of the double-gated dielectric modulated field effect transistor's bio-sensing capabilities being modeled.

To begin the discussion, it is important to describe the general physics involved in the bio-sensing operation of this proposed double-gated dielectric modulated field effect transistor device, which will connect to many of the principles further discussed in the literature review chapter.

The synopsis is that biomolecules, or target analytes which bind to the receptor, have varying permittivities or relatively varying differences in how much electrical energy is stored under the influence of an electric field in a dielectric, such as a nanogap, as an example. This is especially different when compared to the permittivity of a vacuum or free space, such that the material's permittivity will purport an affected change on the dielectric constant and thereby the capacitance. The dielectric constant is mathematically referred to as the ratio of the material's permittivity, which is the analyte in this application, to the permittivity of a vacuum in which, for example, a nanogap is completely empty.

As the analyte hybridizes to the binding receptor, the permittivity not only changes, impacting the dielectric constant, but also a bias is imparted, if the targeted analyte is charged, which influences the electrical properties within the channel by direct influencing of the driving gate. This can change the current carrying capacity within the channel or change the active mode current, in addition, to the threshold voltage can be fluctuated, when the activity or bias is imparted on the bulk of the material for a double-gated device within the nanogap region, introducing body effect. In addition, if charged biases from the biomolecules, such as DNA, are bound to the source end, body effect will also occur, although in practical designs and applications, the silicon dioxide or whichever layer is being used for the analytes to hybridize to in the cavity often never overlap with the source or drain. This issue may occur if there is a process defect in which the layer used for hybridization overlaps with the source or drain terminals.

The advantage to dielectric modulation is the detection of neutrally charged analytes and charged analytes, as it is based on dielectric constant changes versus charged biases which would not be as influential or detectable with neutral biomolecules, and where the nanogap has the advantage of trapping the target analytes within the cavities. The double- gated configuration further expands upon the sensing range, improving the device performance.

With the nanogap configuration, the biomolecular charges and imparted biases influence the operating characteristics of the inversion layer formation, channel establishment, current-carrying capacity, and other electrical characteristics. In many of the research papers, which will be referred to in the next chapter, the dual gate configuration offers the advantage of improving sensitivity as is the change in threshold voltage when analytes have hybridized.

The design built in the Synopsys Sentaurus software environment will now be referred to as a moment to connect the aforementioned principles of physics and how to optimize a design and to discuss what trade-offs exist when designing for this double-gated dielectric modulated field effect transistor device configuration.

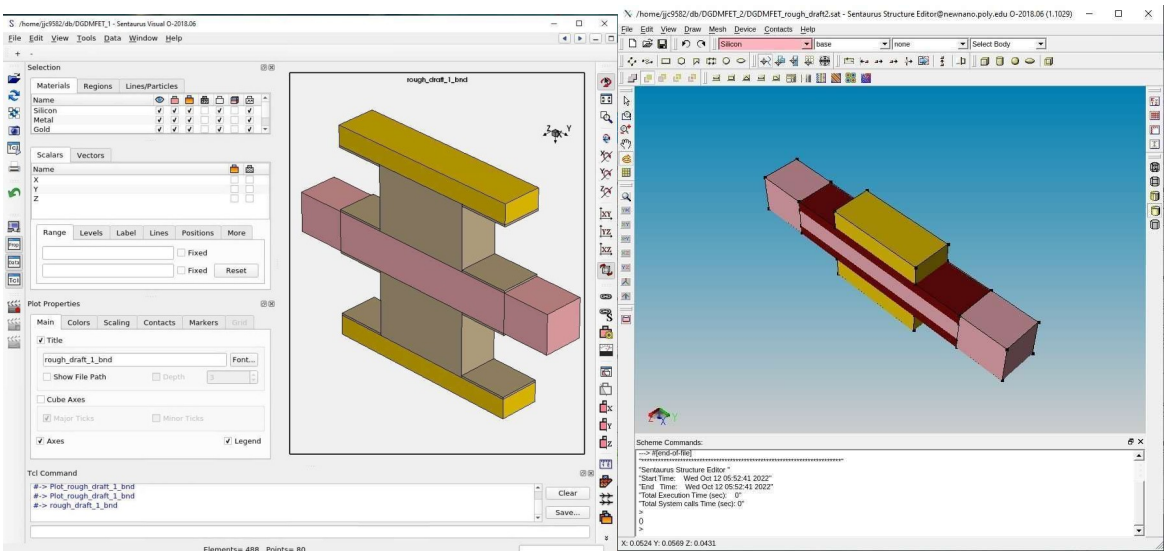

Figure 1. Double-gated dielectric modulated field effect transistors with (left) and without (right) nanogap implementations. The nanogap height is 33 nm which is close to 1/3rd of the 100 nm channel length. The gate thicknesses are 10 nm, and the hybridization layers are 1 nm in thickness. Similar dimensions are employed, without the use of the nanogap or hybridization layers, for the configuration on the right. The hybridization of the analyte is to the gate surface for that topology, in which it was used to compare in terms of sensitivity performance. The literature indicates that

the nanogap implementation and double-gated structure is more advantageous for bio-sensing with superior sensitivity and range.

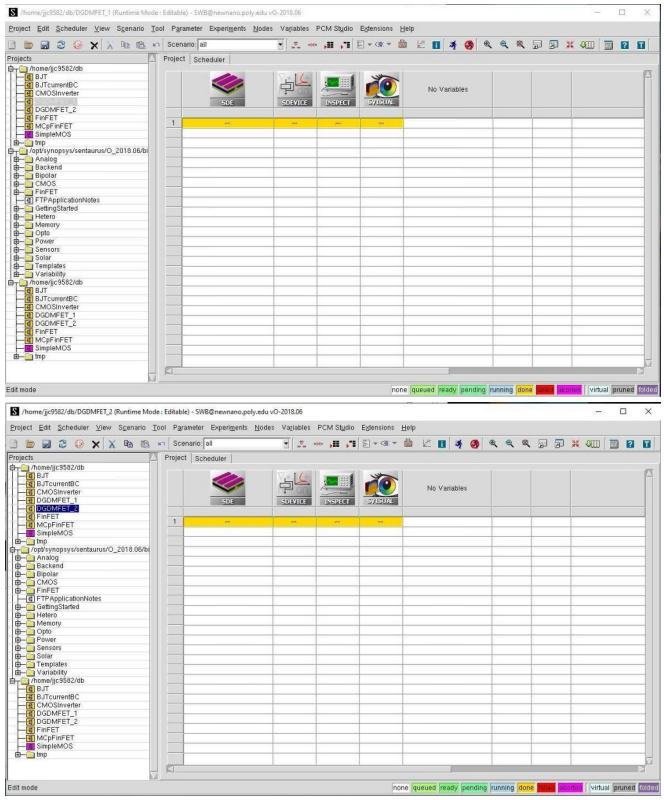

Figure 2. Compilations of the DG-DMFET designs

The software's user interface indicates a successful compilation run of both the design projects. However, even with the template compilations, some data was unavailable or not generated as raw data to be then exported to some other platform. I will discuss or overlap other research findings to provide the expected results of typical double-gated dielectric modulated field effect transistor devices. In addition, the programming files formatted as .cmd files have been provided for each of the stages in the overall pipeline process utilized in the above figure's compilation.

```
Math{
Extrapolate
Derivatives
* Avalderivatives
RelErrControl
Digits=5
ErRef(electron)=1.e10
NaturalBoxMethod
}
Plot{
eDensity hDensity
eCurrent hCurrent
TotalCurrent/Vector eCurrent/Vector hCurrent/Vector
eMobility hMobility
eVelocity hVelocity
eEnormal hEnormal
ErRef(hole)=1.e10
Notdamped=50
Iterations=20
*Newdiscretization
Directcurrent
Method=ParDiSo
Parallel= 2
ElectricField/Vector Potential SpaceCharge
eQuasiFermi hQuasiFermi
Potential Doping SpaceCharge
SRH Auger
AvalancheGeneration
DonorConcentration AcceptorConcentration
Doping
eGradQuasiFermi/Vector hGradQuasiFermi/Vector
eEparallel hEparallel
BandGap
BandGapNarrowing
Affinity
ConductionBand ValenceBand
}
Solve{
NewCurrentFile=""
Coupled(Iterations=100){ Poisson }
Coupled(Iterations=100){ Poisson Electron Hole }
Coupled{ Poisson Electron Hole }
Quasistationary{
InitialStep=0.01 Increment=1.35
MinStep=1e-5 MaxStep=0.2
Goal{ Name="D" Voltage= @Vd@ }
){ Coupled{ Poisson Electron Hole} }
Quasistationary{
InitialStep=1e-3 Increment=1.35
MinStep=1e-5 MaxStep=0.05
```

Figure 3: Sdevice cmd file example, where each plot variable is being invoked for parsing and processing to take place in what would be generated or visible in the inspect and svisual tool interfaces.

```
#-------------------------------------------------------------------#
# Script file designed to compute : #
# * The threshold voltage : VT #
# * The transconductance : gm #
#-------------------------------------------------------------------#
if { ! [catch {open n@previous@_ins.log w} log_file] } {
set fileId stdout
}
puts $log_file " "
puts $log_file " ------------------------------------ "
puts $log_file " Values of the extracted Parameters : "
puts $log_file " ------------------------------------ "
puts $log_file " "
set DATE [ exec date ]
set WORK [ exec pwd ]
puts $log_file " Date : $DATE "
puts $log_file " Directory : $WORK "
puts $log_file " "
puts $log_file " "
# #
# idvgs=y(x) ; vgsvgs=x(x) ; #
# #
set out_file n@previous@_des
proj_load "${out_file}.plt"
# ------------------------------------------------------------------ #
# I) VT = Xintercept(maxslope(ID[VGS])) or VT = VGS( IDS= 0.1 ua/um ) #
# ------------------------------------------------------------------ #
cv_create idvgs "${out_file} G OuterVoltage" "${out_file} D TotalCurrent"
cv_create vdsvgs "${out_file} G OuterVoltage" "${out_file} D OuterVoltage"
#.................................................................. #
# 1) VT extracted as the intersection point with the X axis at the point #
# where the id(vgs) slope reaches its maxmimum : #
#.................................................................. #
set VT1 [ f_VT1 idvgs ]
puts $log_file " "
#.............................................................. #
# 2) Printing of the whole set of extracted values (std output) : #
#.............................................................. #
puts $log_file "Threshold voltage VT1 = $VT1 Volts"
puts $log_file " "
# 3) Initialization and display of curves on the main Inspect screen : #
cv_display idvgs
cv_lineStyle idvgs solid
cv_lineColor idvgs red
```

```
# ------------------------------------------------------------------ #
# II) gm = maxslope((ID[VGS]) #
# ------------------------------------------------------------------ #
set gm [ f_gm idvgs ]
puts $log_file " "
puts $log_file "Transconductance gm = $gm A/V"
puts $log_file " "
set ioff [ cv_compute "vecmin(<idvgs>)" A A A A ]
puts $log_file " "
puts $log_file "Current ioff = $ioff A"
puts $log_file " "
set isat [ cv_compute "vecmax(<idvgs>)" A A A A ]
puts $log_file " "
puts $log_file "Current isat = $isat A"
puts $log_file " "
set rout [ cv_compute "Rout(<idvgs>)" A A A A ]
puts $log_file " "
puts $log_file "Resistant rout = $rout A"
puts $log_file " "
cv_createWithFormula logcurve "log10(<idvgs>)" A A A A
cv_createWithFormula difflog "diff(<logcurve>)" A A A A
set sslop [ cv_compute "1/vecmax(<difflog>)" A A A A ]
puts $log_file " "
puts $log_file "sub solp = $sslop A/V"
puts $log_file " "
### Puting into Family Table #####
ft_scalar VT $VT1
ft_scalar gmax $gm
ft_scalar ioff $ioff
ft_scalar isat $isat
ft_scalar sslop $sslop
ft_scalar rout $rout
close $log_file
#----------------- END ---------------#
```

Figure 4: Code used to plot via the inspect.cmd file, which is intended to generate transfer curve characteristics and information about output impedance, transconductance, etc.

After inputting the above respective cmd files, as just examples of templates used in the process of trying to generate graphical and other forms of data, the simulation profile result below was generated.

Figure 5: Simulation Profile, plots are noted as not generated which has been identical to template projects, which is the intended reason for referencing the literature review, using another CAD software to analytically model the DG-DMFET designs of other research projects for typical results.

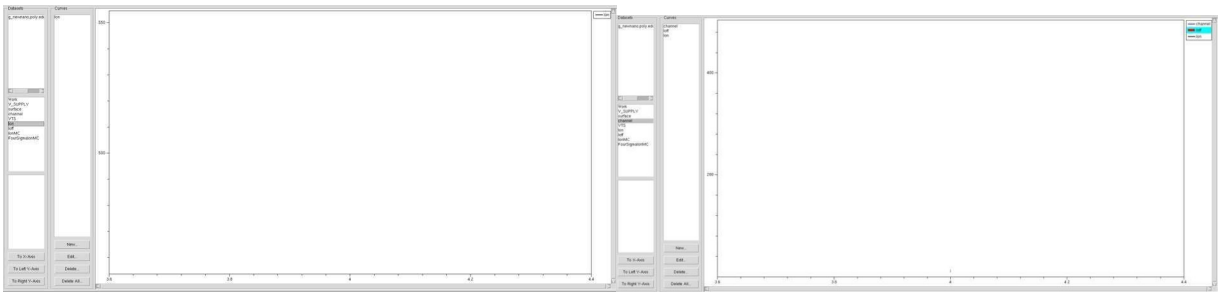

Figure 6: Using the inspect profile to try and generate transfer curve characteristics of an innate tutorial design. The indications on the right column should show the variables that are trying to be plotted with respect to the x axis which is the supply voltage, however, there were

complications in this specific design software among some projects in getting graphical data. The different cmd files which account for measuring and getting data of the variables noted within them were not able to alter the output and achieve generated graphical data. Instead, with some designs, the electron and hole gradients/densities were observable. It is at this end that alternative simulation results would provide an account of what should have vaguely similar output-wise of the compilable DG- DMFET designs. In addition, many designs were only built out of the structural design editor stage such as the following FinFET design example.

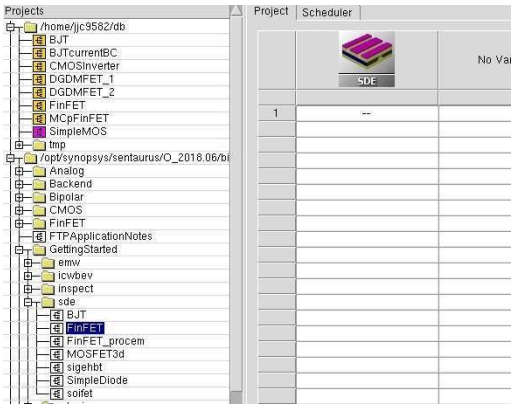

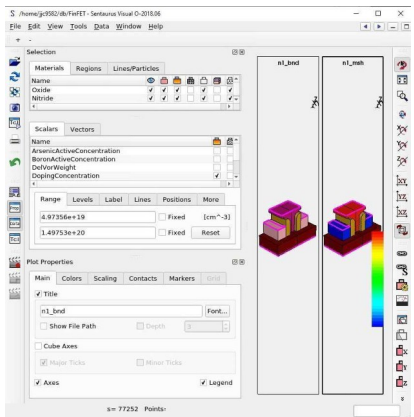

The CMOS inverter example, in the tutorial, also exhibited the same characteristic of not displaying the plot data:

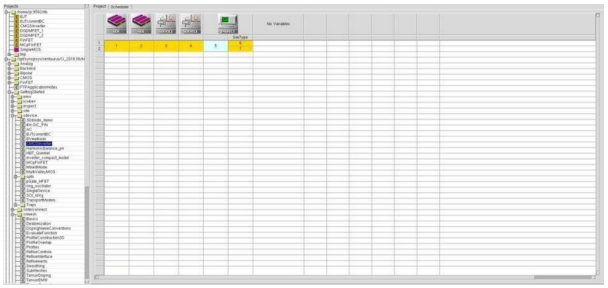

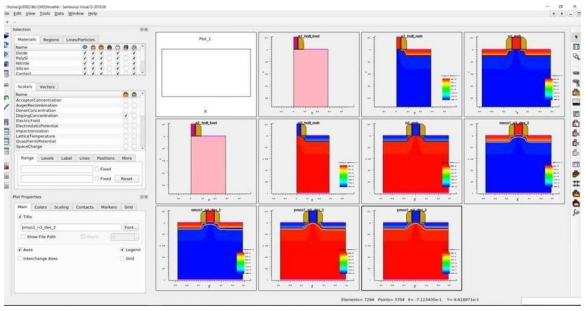

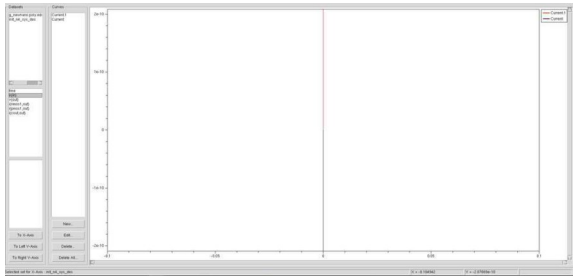

The next topics will be the expected advantages and future work, regarding the design, as well as the theoretical results with comparison to other research designs that would give insight into the transfer curve characteristics.

The expected advantage of the design, being that the nanogap height is 33 nm compared to a channel length of 100 nm, is that there is more optimal gate control, meaning there is less power consumption or need for larger gate voltage to drive the device than if the nanogap were much higher. However, this comes at the cost of sensitivity performance which is an ideal factor to the DG-DMFET design, but not substantial depending on the application. If the application requires greater bio-sensitivity, then it would be more advisable to design a higher nanogap until the optimal point, without requiring excessive gate voltages needed to drive the DG-DMFET. In the literature review, nanogap geometries and materials are proposed to determine the most ideal geometry and material composition for the device's performance. In accordance to these considerations discussed in the literature, the material composition would be changed such that the gates would be gold, for the improved conductivity and gate control, in order to offset the mitigation that comes with an increased nanogap height for higher sensitivity, and the I-beam structure, which constitutes the cavity for the analytes to hybridize to, would be silicon dioxide for its optimal increase to sensitivity, evidenced by the literature research.

In the future circumstances, it would be important to make these updates as well as to consider, in the most ideal scenario licensing-wise and otherwise, using Silvaco TCAD or another TCAD for the design simulations potentially in tandem with Sentaurus. As evidenced previously, the built-in examples experienced some issues with plotting and analytical modeling, which might not always be the case. In addition, since this design is specifically dual-gated and the cmd files are programmed and formatted with one gate terminal as a section, another TCAD may be more optimal in analytically modeling the dual-gate structure.

As per an example of expected results of DG-DMFET characteristic curves, the following figures represent the device structure and its respective curves, observed in the research article “A Device Simulation-Based Investigation on Dielectrically Moulated Fringing Field-Effect Transistor for Biosensing Applications” conducted by S. Kanungo, S. Chattopadhyay, K. Sinha, P. Gupta, and H. Rahaman, whose work was published in the IEEE Sensors Journal in 2017.

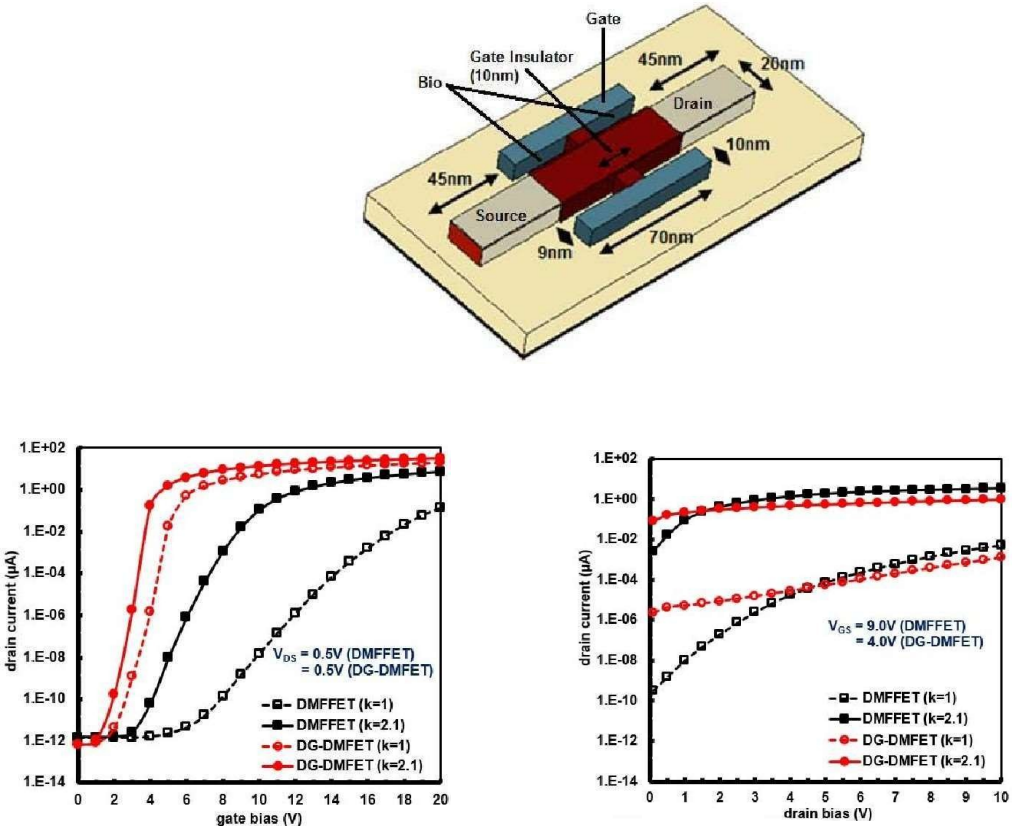

Figure 7: Relatively similar design(with dimensions specified) for an understanding of expected behavior when it comes to transfer characteristic curves

The expected current carrying capacity that the device can have is around 60-80 micro amperes, with ranges as low as in the nano-amperes and femto-amperes with less gate drive, and this design does not have an especially high nanogap relative to the channel length, thereby providing better gate control performance, which is better for applications where

power consumption is more important and where bio-sensitivity is not as crucial.

Next, the nanogap height increase will be considered with respect to the transfer curve characteristics of the DG-DMFET, in order to get an expectation of the behavior with the aforementioned changes applied. In order to get this idea, the research paper “Analytical Modeling of Sensitivity Parameters Influenced by Practically Feasible Arrangement of
Bio-Molecules in Dielectric Modulated FET Biosensor”, conducted by the team of Rahul Das, Ankush Chattopadhyay, Manash Chanda, Chandan K. Sarkar, and Chayanika Bose, will be referred to and further explained in the literature review. Below are the transfer curve characteristics and purported designs with their respective biomolecular patterns to describe the influence of occupation within the heightened nanogap cavity.

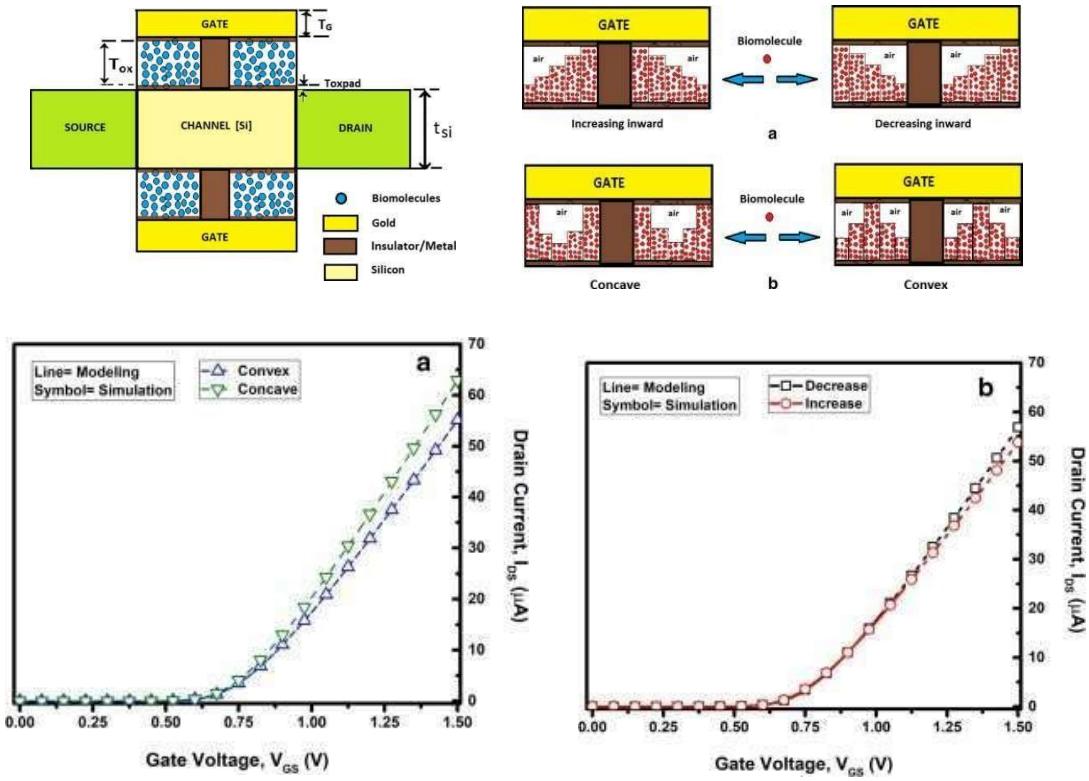

Figure 8: Another example of a DG-DMFET design and its respective transfer curve characteristics with respect to various biomolecular patterns within the nanogap cavity.

A plot of the drain current vs drain-source voltage is not available, however, it shows a similar range of current carrying capacity, and the graph implements a lower range of bias voltages on the gate, with sufficient gate control to get out of the cut-off region. Both the graphs are comparable in terms of this aspect, where less swing at the gate is needed to operate the transistor, thereby it is a smart decision to optimize the nanogap height for improved sensitivity, as it will not impact the transfer curve characteristic drastically in terms of not only this, but also in terms of the current carrying capacity, where the transistors' dimensions are similar to the proposed design of this chapter.

Since the proposed design is similar in scale and similar architecturally to the former examples referred to, the literature has provided similar examples to infer how the proposed design would behave in terms of its transfer characteristics, analytical modeling, and general simulation.

To conclude this chapter, the general knowledge of the device physics, operation, expected advantages, insights into the design and its impact on performance, as well as the future decision making into improving this chapter's proposed design– all of these topics will be valuable points of detail in further understanding the upcoming chapter– the Literature review, examining and evaluating influential and modern physics and knowledge into the design making process of DG DMFETs.

Double-Gated Dielectric Modulated Field Effect Transistors and their Modeling as Biosensors, a Literature Review and design built in the Sentaurus Software Environment

Chapter 2 – Literature Review

This chapter's intent is to document and to discuss the important scientific research findings that regards the implementation, practice, and theoretical physics of the doubled-gated dielectric modulated field effect transistor device. The general procedure of this literature review is to sequentially examine each papers' findings, conclusions, and contributions to the field of study, in which the order is identical to this works' bibliography section.

The analysis begins with the following research paper, "Analytical Modeling of Sensitivity Parameters Influenced by Practically Feasible Arrangement of Bio-Molecules in Dielectric Modulated FET Biosensor", conducted by the team of Rahul Das, Ankush Chattopadhyay, Manash Chanda, Chandan K. Sarkar, and Chayanika Bose.

The paper concerns the analytical modeling of a dielectric modulated double-gate field effect transistor, purposed for biosensing applications, and discusses the impacts of nanogap geometry and biomolecular arrangement in these cavities on the sensor's sensitivity to pick up on these biomolecules' imparted changes on the dielectric constant in the current- voltage characteristic curves. Other important factors are examined such as probe placements, as the biomolecular arrangement and steric hindrance may affect the device performance. With the design of nanogaps comes the inclusion of additional capacitance factors to the modeling, in addition to those purported by the biomolecules occupying the nanogap cavities. The researchers examine all of these factors and have derived, with this capacitance model, the threshold voltage, drain current, and sensitivity variations purported from the device architecture/ geometry.

The data and results of these researchers were achieved via the TCAD device simulator, simulating the device physics and characteristics upon the device geometry and the biomolecular interactions contained within the nanogap cavity.

A main advantage of the use of dielectric modulated field effect transistors for biosensing applications is in the detection of charged and neutral biomolecules, the sensitivity factor can be equivalent, in addition to having higher sensitivity and lower manufacturing costs than non-FET-based biosensors. Another major advantage of the DMFET specifically is that its gate capacitance is influenced by the dielectric constant changes emerging from the purported changes from biomolecular interactions such as binding to analytes. The dielectric modulated field effect transistor experiences variations in the threshold voltage and drain current, based on the dielectric constant changes, even without the influence of activities within the nanogap, meaning it can be air-filled or vacuous with this intended effect.

As per the device production/manufacturing, basic 3D structures of dielectric modulated field effect transistors with the nanogap architecture has been implemented via the use of thin film deposition and subsequent wet etching, in order to reduce lithographic complications for planar nanogap field effect transistors.

There are different architectural proposals to optimize the sensitivity of the nanogap dielectric modulated field effect transistors, and one of the major proposals to optimize the sensitivity is to implement a dual-gate topology. The implementation of two nanogaps would allow for more biomolecules to be trapped within the device’s cavities, and the intended effect is to increase the sensing range. The research team notes the work of Narang and company, who have proposed a DG-DMFET device structure and whose work will also be referred to as a part of this literature review. The device structure is given in the following figure. This double-gated dielectric modulated field effect transistor employs a modulated nanogap embedded gate insulator, where the silicon dioxide layer beneath the gate has

hydroxyl groups to hybridize to the biomolecule receptors in this model. The research team determined that there was better performance, in terms of sensitivity and operation, with the use of a 1 nm silicon dioxide layer on the top of the nanogap.

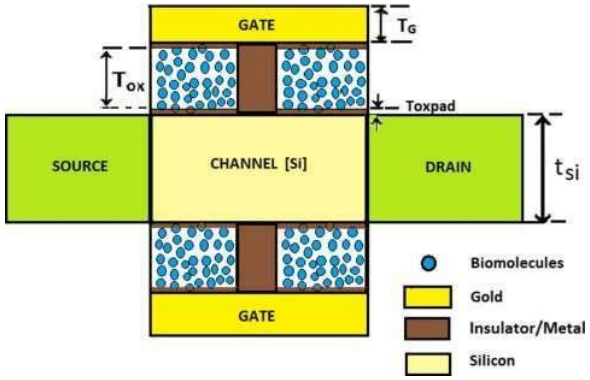

The research team analytically modeled biomolecule-filled nanogaps in the double gated dielectric modulated field effect transistor, with the inclusion of sensitivity optimization as a result of surface functionalization, the process in which biomolecules hybridize to the bulk material, silicon dioxide for this particular device structure. The modeling covers surface potential, threshold voltage, drain current, and sensitivity as parameters influenced by the biomolecule-filled nanogaps in between the front and back gates and the channel. Another important factor that is considered, in this analytical modeling, is the biomolecular orientation that is occupying the nanogap cavities, which is examined in four distinct manners- increasing inward, decreasing inward, concave, and convex. This is demonstrated in the figure below:

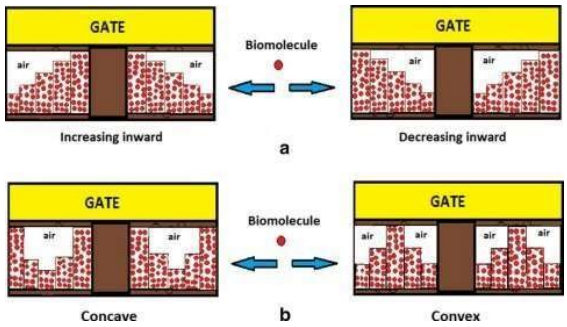

In this research article, the researchers performed a comparative analysis, using three materials as the dielectric layers, with the consideration of varying biomolecular permittivities which would impact the threshold voltages and current sensitivities of the different device topologies/material compositions. The researchers compare different biomolecular materials as ligands to be received for the analytical modeling of the biosensor, in which they compare the sensitivity increases based on the biomolecules' permittivity constant k. The researchers examined the impacts of biomolecular permittivities in the three different material compositions for the device's nanogap. The silicon dioxide material was decided as the most optimal for higher sensitivity, because, of the three nanogap materials, it reported the largest changes in threshold voltage. For the impact on the active current change, silicon dioxide had comparable values for the lower permittivity k biomolecules, but had a better performance standard for the higher permittivity biomolecules with k = 22, as indicated by the figures below.

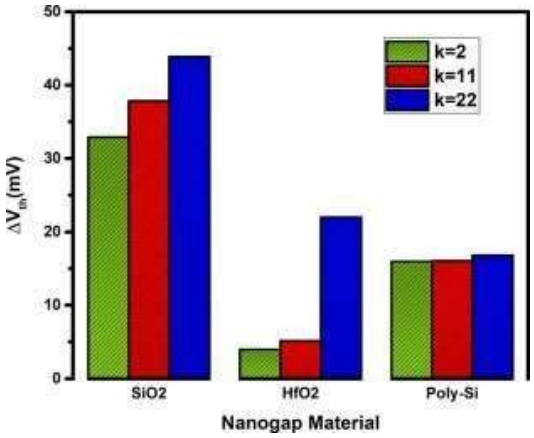

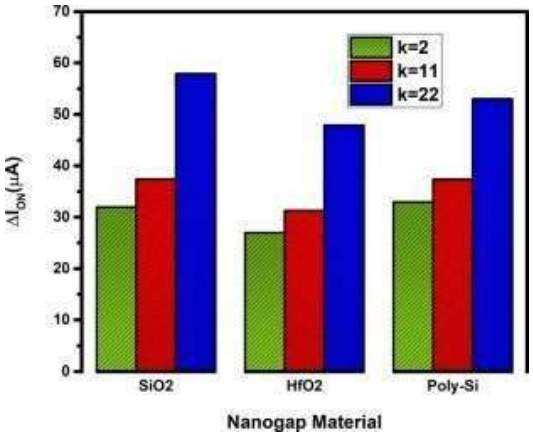

With the higher reported change in the threshold voltage, and comparable active current change for all other k except for 22 when it is higher, the silicon dioxide nanogap material is optimal for improving device sensitivity.

The next parameter the research team looked into is the optimal geometry for the nanogap structure, in order to optimize the biosensor's sensitivity. What was determined is that larger nanogap heights correspond to poorer gate control due to greater spatial separation. In addition, higher

permittivities of biomolecules corresponded with larger active currents and greater active current sensitivity. To address the former point, with larger height nanogaps, a larger gate-source voltage is needed to drive the device outside of cut-off than the alternative of a shorter nanogap height. However, with the larger nanogap height, it was found that threshold voltage sensitivity increased. It was observed that a nanogap from 25 to 40 nm decreased the change in active current by -15%, which is due to the increase in length between the gate and the channel, whereas the impact on the change in threshold voltage was 2 times greater. The researchers determined that for this trade-off, there was a greater performance overall for the sensitivity with having a much greater change in the threshold voltage. The following figure demonstrates the impacts of the nanogaps' height and width dimensions on the change in the threshold voltage.

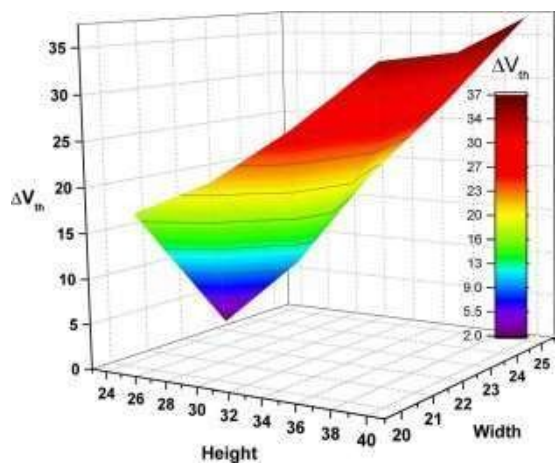

In order to model the surface potential, the research team characterized the two-dimensional potential profile of the channel with Poisson's equation:

$$\frac{\partial^2\psi(x,y)}{\partial x^2} + \frac{\partial^2\psi(x,y)}{\partial y^2} = \frac{qN_a}{\epsilon_{si}}$$

The electric field at the top channel was characterized as:

$$\left.\frac{\partial\psi(x,y)}{\partial y}\right|_{y=0} = \frac{C_{ox}(\psi_1(x) - (V_{GS} - \phi_{fb}))}{\epsilon_{si}} = P_2(x)$$

Whereas, the electric field at the bottom channel was characterized as:

$$\left.\frac{\partial\psi(x,y)}{\partial y}\right|_{y=t_{si}} = \frac{C_{ox}((V_{GS}-\phi_{fb})-\psi_1(x))}{\epsilon_{si}}$$
$$= P_2(x) + 2t_{si}P_3(x)$$

The expression of the potential function was able to simplified into the following expression, because of the symmetric properties of the device where the potentials are identical in the shorted gate mode:

$$\psi(x,y) = \psi_1(x) + \frac{C_{ox}}{\epsilon_{si}}\{\psi_1(x) - (V_{GS}-\phi_{fb})\}y$$
$$- \frac{C_{ox}}{\epsilon_{si}t_{si}}\{\psi_1(x) - (V_{GS}-\phi_{fb})\}y^2$$

Via the analytical modeling process, the variations in the threshold voltage change and active current change were determined with their respective corresponding nanogap widths and heights.

Width (nm)	Height (nm)							
	25		30		35		40	
	ΔV_{th}	ΔI_{ON}	ΔV_{th}	ΔI_{ON}	ΔV_{th}	ΔI_{ON}	ΔV_{th}	ΔI_{ON}
20	17	42.7	21	40.1	27	37.7	34	35.6
22.5	2	45	10	42.2	23	38.5	34	38
25	11	51.2	18	48.5	27	46.1	37	43.7

It is indicated, from this table, that the largest change in threshold voltage occurs when the nanogap geometry is a height of 40 nm and width of 25 nm, whereas, for the larger change in active current, the nanogap geometry has a height and width of both 25 nm, a 1:1 ratio. As mentioned before, the benefits of increasing the nanogap height allows for a much greater change in threshold voltage change than the depreciation in active current change, however, the requirement, since there is less gate control, is to drive with a larger gate-source voltage.

Next, it is important to discuss the estimated capacitance corresponding to a nanogap which is practically filled with different biomolecules with varying capacitances and not completely filled or uniform, hence why the research team has modeled the nanogaps in the previously noted 4 patterns. The researchers determined an equivalent capacitance expression and figure to note the nanogap as the following:

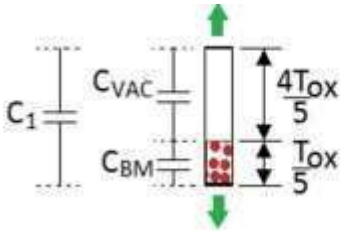

Area = α_1

$$C_{BM} = \frac{5k\epsilon_0\alpha_1}{T_{ox}}; \quad C_{VA} = \frac{5k_v\epsilon_0\alpha_1}{4T_{ox}}$$

$$C_1 = \frac{C_{BM}C_{VA}}{C_{BM} + C_{VA}} = \frac{5kk_v\epsilon_0\alpha_1}{T_{ox}(4k + k_v)}$$

Cbm refers to the capacitance purported by the biomolecules which are only partially filling the nanogap cavity, whereas the Cva is the vacuous or other filling space's associated capacitance. Since they are connected in series, the C1 expression is used to signify the capacitance within the channel, which is represented as Cz in the following graph which shows additional capacitances noted in the nanogap structure.

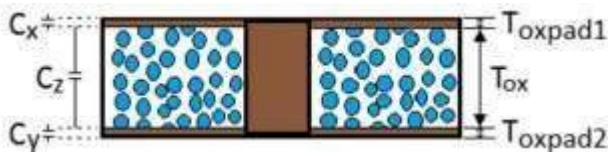

In the situation of increasing or decreasing patterns within the nanogap, each height is treated as its own respective column, as each biomolecule height has its own step size. Please refer to the figure showing the four nanogap cavity occupations, and it will be shown, from the figure, there are 5 distinct columns with different biomolecular heights. For each column, there is a different unique capacitance which is mathematically expressed as the following: $C_{col} = \epsilon_{ox1}\alpha_{col}/T_{ox}$ where alpha represents the total area associated with the column in the nanogap. From each column's derivation, the Cbm from earlier can be calculated and then used to derive the overall capacitance in between the nanogap which is referred to as Cz once again in the figure above. This similar philosophy can be applied to determining the aforementioned factors of the concave and convex patterns within the nanogap.

It is appropriate to expound upon bio sensitivity and the factors impacting it. Firstly, the sensitivity factor describes the threshold voltage change with the target biomolecules bound or contained within the nanogap cavities. The threshold voltage change, moreover, is the threshold voltage without any activity in the nanogap minus the threshold voltage with biomolecules

contained within the nanogap cavities. The bio sensitivity can then be mathematically defined as this difference or change divided by the threshold voltage without any activity. Factors that impact the sensitivity include biomolecule size, occupation of the nanogap, nanogap height and width, and the permittivity of the biomolecules. Previously discussed was the allowance of more biomolecules to bind and be contained within the nanogap with larger nanogap heights, showing a direct relationship with nanogap height and sensitivity. Furthermore, there is an ideal biomolecule size and permittivity to improve the sensitivity factor, however, this depends on the device geometry as well such that the nanogap can optimize its allowance of the target molecule within the nanogaps.

The research team obtained results from the modeling and simulations via Silvaco TCAD, implementing a fully filled nanogap with varying biomolecular patterns for the dielectric modulated double-gated field effect transistor. The transfer characteristics curves are provided below.

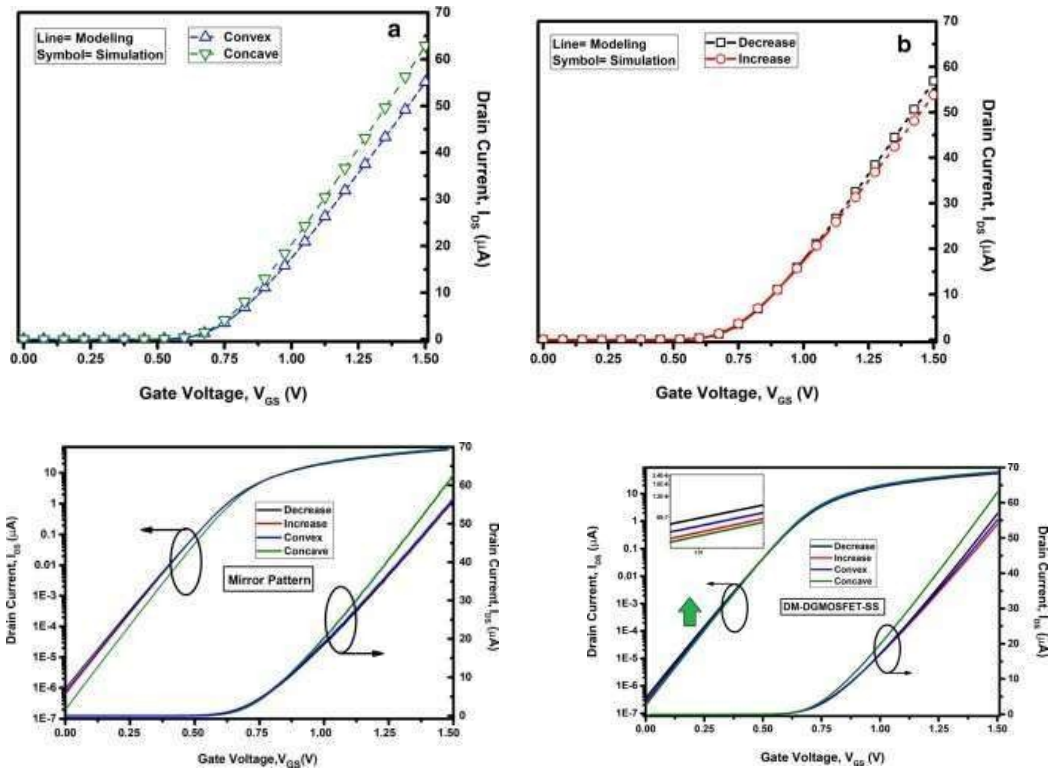

The concave pattern displays the largest active current as well as the smallest off current. These transfer curve characteristics exhibit more of the practical application, in which realistically the nanogap is not fully filled nor does it have a uniform distribution within the nanogap. The mirror is noted as the pattern within the nanogap as if it were flipped at the x axis to present the mirror image of the biomolecular content contained within the nanogap. The mirror pattern curves are simulated as well, in which the concave pattern exhibits the lowest off current and highest active current as well. The figure below demonstrates the pattern of the a) mirrored structure and b) same structure.

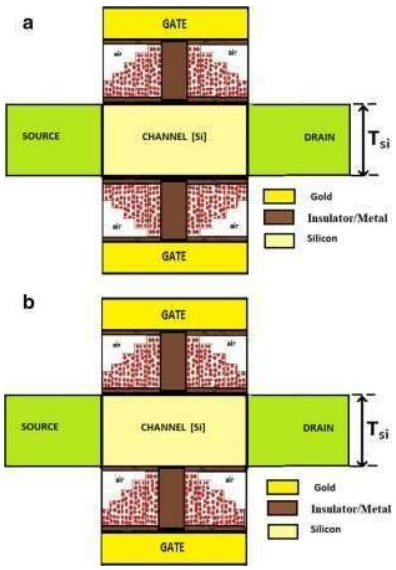

The research team documents the differences between the mirrored pattern and the same structured pattern for the nanogaps in terms of the change in the threshold voltage change, indicating sensitivity, as well as the active current change.

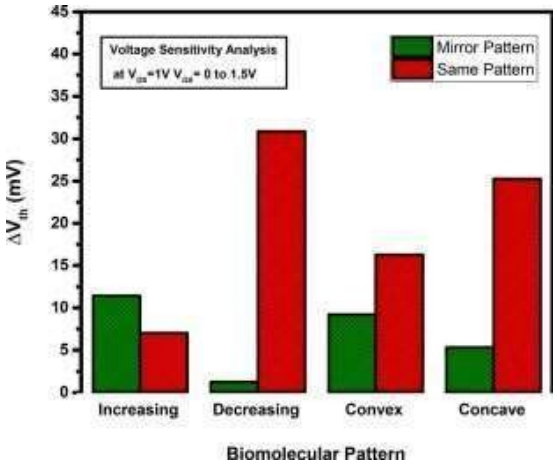

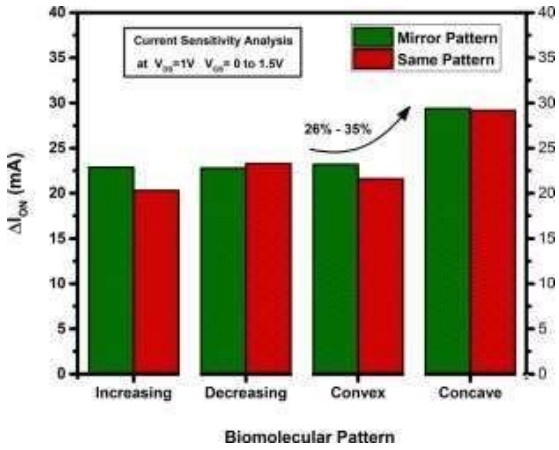

The research finding is that the decreasing pattern with the same pattern for the top and bottom nanogaps resulted in the largest change in threshold voltage, which means that it has the greatest bio sensitivity. For the mirrored convention, the threshold voltage change or sensitivity was highest for the increasing pattern.

With respect to the change in the active current, the concave pattern resulted in the largest outcomes for both the mirrored and same structured patterns of the top and bottom nanogaps. In addition, the relative changes among these topologies was not as significant among different patterns, with the exception of the concave pattern, and especially when comparing the mirrored structures to the same structured patterns for the top and bottom nanogaps. Whereas, for the change in threshold voltage or sensitivity, the differences between the mirrored and same patterns was a lot larger, in addition to the varying differences between different biomolecular patterns.

The research team accounts for the potential confounding effects of steric hindrance, probe placement, and fabrication errors, which impact the nanogap’s ideal situation of fully containing its target molecules. The deviations are then measured as errors when comparing to a fully filled nanogap cavity, in the following figures.

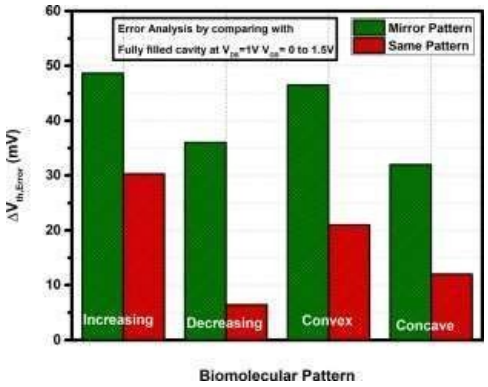

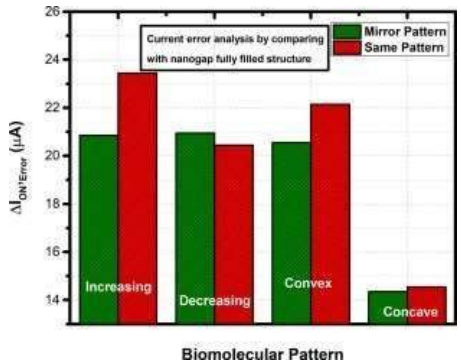

The conclusion is that the same pattern for the top and bottom nanogaps results in a significant magnitude decrease in error, when compared to the mirror pattern configuration. The same pattern structure has a slightly larger error than the mirrored pattern convention, with respect to the active current change error. Since this difference is marginal and sensitivity is an extremely important factor to the practical application of a biosensor, the same pattern configuration is considered a better design choice. The research has found that the dielectric modulated double-gated field effect transistor with the same pattern for the top and bottom nanogaps outperforms the mirrored pattern, as well as the concave pattern being the most effective biomolecular pattern among the same pattern DG-DMFETs.

The analytical modeling and research has shown the DM-DG MOSFET-SS with the concave biomolecular pattern to have the best performance, as it has the best sensitivity and a very proficient error analysis. With the optimal nanogap height aforementioned, the sensitivity performance is the best of all the topologies noted in this study.

The fabrication process of the DG-DMFET employs an extremely precise wet etching procedure, however, process variation or defects can occur and influence the design performance. The researchers note four possible structural variations emerging from the wet etching process. The situations are when the nanogaps are wider in the drain side for both the top and bottom gates, when the nanogaps are wider in the source terminal for the top and bottom gates, when the nanogaps are wider in the drain terminal

for one gate, and when the nanogaps are wider in the source terminal under one gate.

The figures below indicate the impacts of these process variations on the change in threshold voltage and the change in the active current.

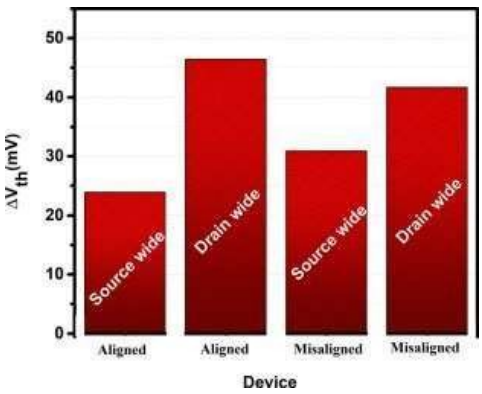

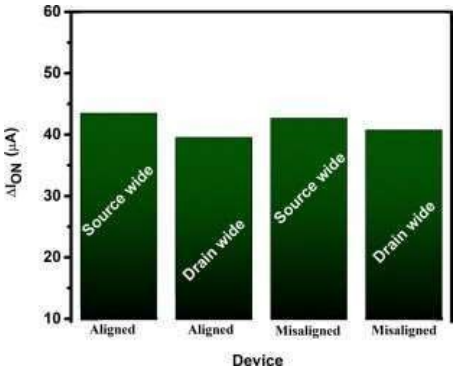

The change in the sensitivity analysis from these process variations are listed in the table below.

Device		V_{th} ($k = 11$) (mV)	I_{ON} ($k = 11$) (μA)	V_{th} ($k = 1$) (mV)	I_{ON} ($k = 1$) (μA)	ΔV_{th} (mV)	ΔI_{ON} (μA)
Aligned	Source wide	306.12	74.07	282.21	30.58	23.91	43.49
Aligned	Drain wide	319.97	72.86	273.51	33.34	46.46	39.52
Missaligned	Source wide	311.7	73.94	280.8	31.27	30.9	42.67
Missaligned	Drain wide	318.42	73.34	276.7	32.6	41.72	40.74

To conclude the review of this study, the research team analytically modeled varying dielectric modulated double-gated field effect transistors, determining the optimal biomolecular pattern, structure architecture and geometry, nanogap material, patterns for the top and bottom nanogaps, and other important factors when comparing these different designs to find the most optimal biosensor variation. The paper discusses the important practical factors of the design, such as the realistic equivalent capacitance of the nanogap, sensitivity gains based on biomolecular pattern and structural and material compositions and geometries. The transfer curve characteristics and other analytical modeling and graphs demonstrate the influence of these design factors on the device performance.

The next research paper that will be reviewed is “A detailed investigation of dielectric-modulated dual-gate TMD FET based label-free biosensor via analytical modeling”, conducted by researchers Monika Kumari, Niraj Kumar Singh, and Manodipan Sahoo. The research indicated that FET- based biosensors with one-dimensional nanowires and CNTs as the channel material are more advantageous than label-based detection, due to better electrostatic interactions between the channel and the analytes. The limiting factor is that these structures are difficult to fabricate and are expensive to produce.

The researchers proposed dual-gated TMD-FET based biosensors, represented below.

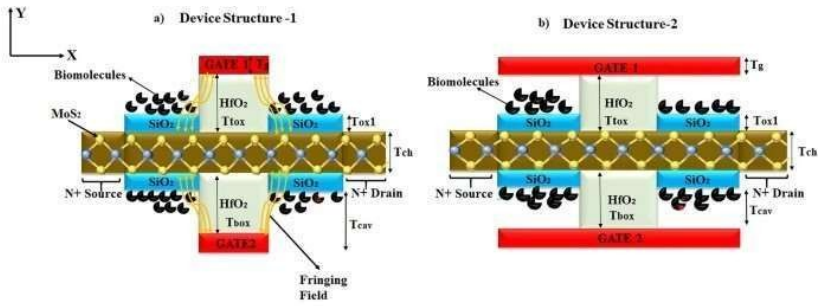

(**a**) Device structure-1 of dielectric-modulated, dual-gate, TMD FET (DM-DG-TMD-FET)-based Biosensor, and (**b**) Device structure-2 of DM-DG-TMD-FET-based biosensor.

The researchers proposed the following production process of the device.

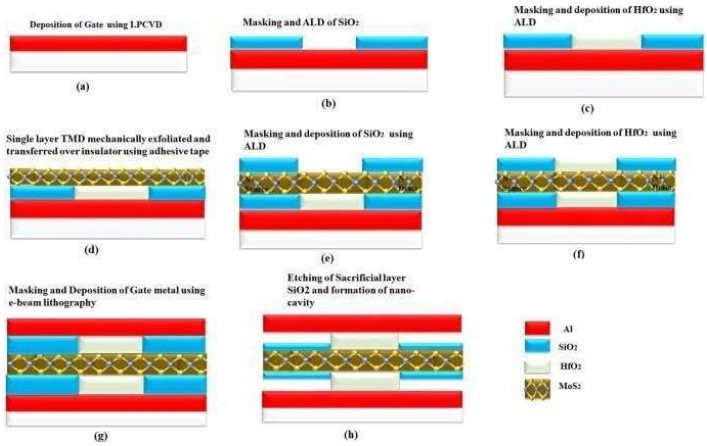

The next discussion is the findings of the Silvaco TCAD simulations, in which the characteristics of the DM-DG-TMD-FET based biosensors were

analytically modeled for their sensitivity and drain current. The characteristics are compared to Nam, H. et al. with regards to their research on MoS2 transistor biosensors.

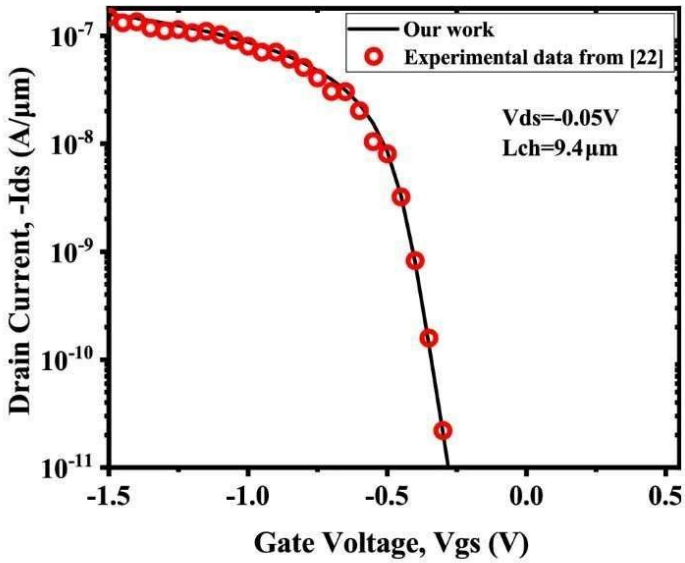

Drain current, (I_{ds}) versus Gate to source bias, (V_{gs})) for back-gate, (Vgb) − 40 V and drain to source bias, V_{ds}= − 0.05 V with channel-length, L_{ch} = 9.4 nm, front and back gate oxides are ZrO_2 $T_{tox} = 17.5$ nm, $k_{tox} = 12.5$ and SiO_2 ($T_{box} = 270$ nm, $k_{box} = 3.9$) respectively.

The researchers investigated the impact of neutral biomolecules and charged biomolecules on the sensitivity, drain current, and surface potential. Among the device structure 1, aforementioned, there was reported to be fringing capacitance influencing the surface potential, where the nano-cavity regions exhibit surface potential changes, unlike the region without the nano-cavity.

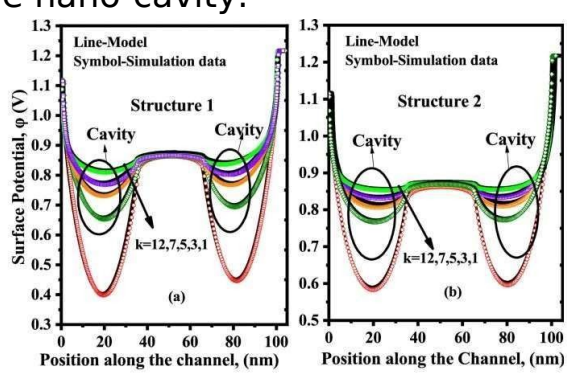

Surface potential of the proposed DM-DG-TMD-FET-based biosensor for (**a**) Device structure-1 and, (**b**) Device structure-2 with different dielectric constants ($\kappa = 1, 3, 5, 7, 12$) of biomolecules. ($V_{gs} = 0.1$ V, $V_{ds} = 0.1$ V $N_f = 0$).

The researchers then plotted the threshold voltage and sensitivity as a function of the dielectric constant, considering that an empty cavity meant

low gate capacitance and a higher driving voltage necessary for electrons to move from the source and into the channel.

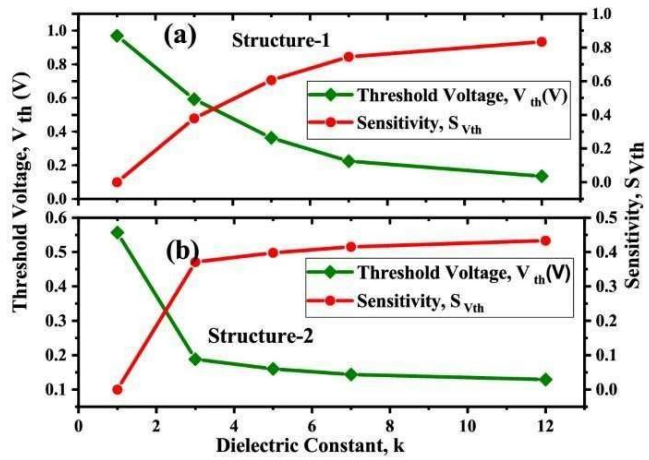

Threshold voltage and Sensitivity w.r.t to dielectric constant (κ) of biomolecules with for Device structure-1 and Device structure-2 ($V_{gs} = 1.2$ V, $\kappa = 5$, $N_f = 0$).

If the dielectric constant is greater for the biomolecules, then gate capacitance and fringing field capacitance increase, thereby impacting the surface potential within the nanogap. The research indicates that this increase results in the fringing field effect dominating, where the surface potential barrier is reduced. If the gate is over the cavity, then fringing capacitance is not dominant in that region, which also allows for better gate control.

Another finding of the research is that the threshold voltage decreases when the dielectric constant increases, and, as an example, when the cavity is empty or completely vacuous such that the permittivity is solely free space, hypothetically, that is when threshold voltage will be at its highest, considering that the k is at its smallest or equal to 1. The researchers also determined the threshold voltages for both the proposed structures, with this condition, as 0.969 V and 0.569 V for structures 1 and 2 respectively.

A sweep was performed to determine the transfer curve characteristics, Id vs Vgs, with varying dielectric constants, for both the topologies.

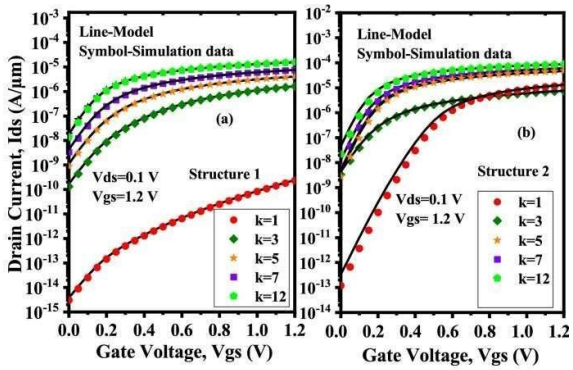

Variation in drain current w.r.t to gate bias for (**a**) Device structure-1 and (**b**) Device structure-2 ($V_{gs} = 1.2$ V, $V_{ds} = 0.1$ V, dielectric constants, $\kappa = 1, 3, 5, 7, 12$, $N_f = 0$).

In addition, the researchers analytically modeled the impacts of the biomolecular charge within the cavity on the threshold voltage and the sensitivity, which were at the lowest for neutral or non-charged analytes.

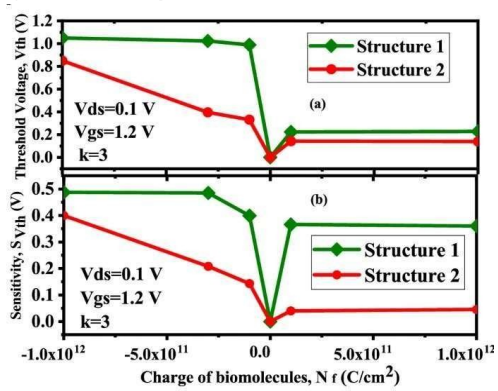

Threshold voltage and Sensitivity w.r.t to negatively and positively charged biomolecules for Device structure-1 and Device structure-2 ($V_{gs} = 1.2$ V, $V_{ds} = 0.1$ V for $\kappa = 3$).

Similar to the previous literature, a sensitivity analysis was performed with variations in the nanogap height and found the same tendency of higher nanogap heights in their improved sensitivity. However, in addition, the dielectric constant is noted as well, sharing a similar trend as theoretically expected from the sensitivity performance.

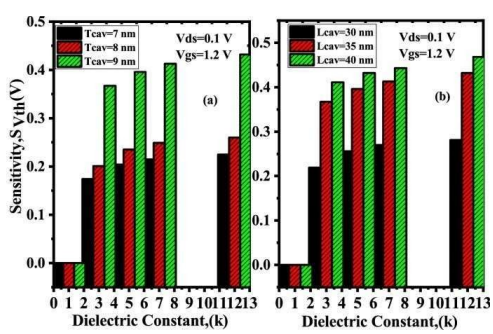

Sensitivity of the device for (**a**) Variation in cavity thickness (**b**) Variation cavity length ($V_{gs} = 1, 2$ V, $V_{ds} = 0.1$ V, $\kappa = 5$, $N_f = 1 \times 10^{11}$ C/cm^2).

The important factor that is being considered, which was mentioned in the previous paper, is the sensitivity changes due to steric hindrance. The occupied biomolecules within the cavity will block the entry of other biomolecules from hybridizing to the receptor. In some situations, the occupation may not be ideal to maximize interactions between analytes and receptors, affecting the effective sensitivity range. This study and research team utilizes the similar biomolecular patterns to the previous study, measuring the dielectric constant for both structures' topologies.

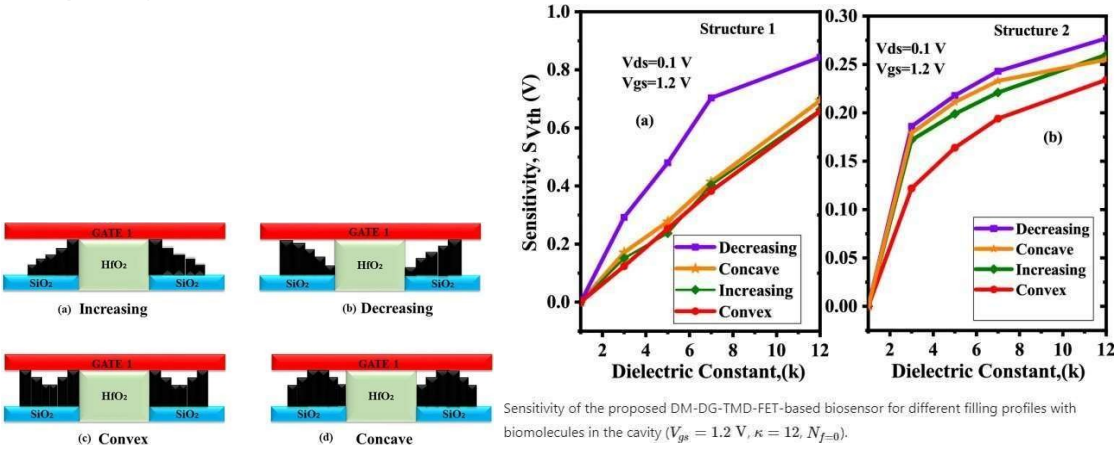

Sensitivity of the proposed DM-DG-TMD-FET-based biosensor for different filling profiles with biomolecules in the cavity ($V_{gs} = 1.2$ V, $\kappa = 12$, $N_{f=0}$).

The sensitivity seems to indicate that for the proposed DM-DG-TMD-FET based biosensors that the decreasing biomolecular pattern yielded the best overall sensitivity for both devices, where device 2's structure is less impactful compared to device 1's. The important factor considered is the inclusion of fringing effects in this model, as well as there being a different material composition which influences the bandgap, and there is inclusion of transition metal dichalcogenides, which differentiate, as a two dimensional semiconductor material, due to its high electron mobility, surface-volume ratio, high electron mobility, charge sensitivity, and other physical properties.

The researchers analytically modeled a MoS2 based dual gated TMD fet biosensor, observing the channel's surface potential, transfer characteristics, dielectric variations within the nano-cavity, as well as observing the impact of steric hindrance and biomolecular patterning within the nano-gap to impact the device's performance. The advantage of this design is in its enhanced sensitivity and label-free detection which is useful

for when there is a lower concentration, so that the device is more able to pick up on the presence of the target analyte from this high-sensitive application.

The next research article that will be discussed is “Investigation of Dielectric-Modulated Double-Gate Junctionless MOSFET for detection of biomolecules”, conducted by the researchers Ajay Singh, Mridula Gupta, Rakhi Narang, and Manoj Saxena. The researchers propose a dielectric-modulated double-gate junctionless MOSFET as a biosensor for the label free detection of biomolecules. In the device simulations, characteristics such as surface potential, electric field, energy bands and drain current are evaluated via analytical modeling.

The rationalization of this design choice is immunity from short-channel effects and improved sensitivity and performance. For the analytical modeling, the researchers simulated the design via the Silvaco Atlas software. The proposed structure is as follows:

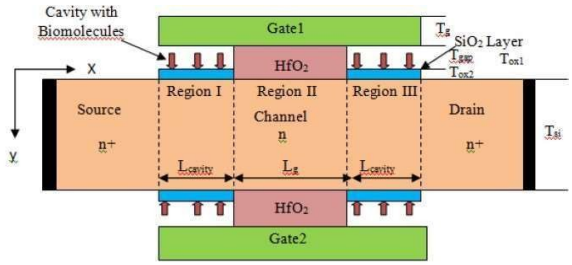

Schematic of DM-DG-TFET with biomolecules in the cavity. Other parameters are considered such as, t_{ox1}= 10nm, t_{ox2} = 1nm, t_{si} = 20nm. Doping in source and drain $N_d = 1x10^{26}m^{-3}$, and channel is $N_d = 1x10^{25}m^{-3}$.

Using the model above, the researchers determined the surface potential distribution without the cavity and after the cavity is formed with immobilized neutral and charged analytes within it.

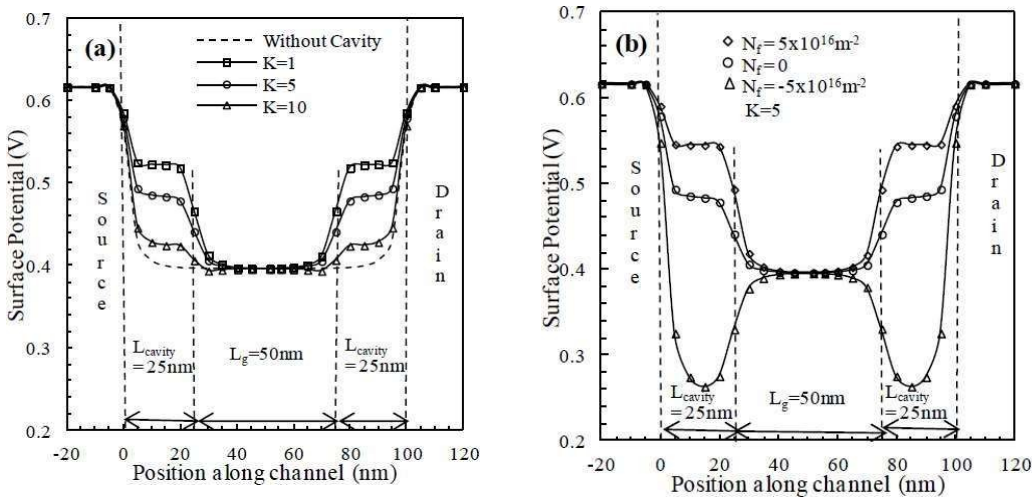

The observation to be made, when it comes to neutral biomolecules within the cavity, is the increase in the surface potential, when the cavity exists and with a vacuous free space permittivity, allowing for the overall dielectric constant to equal 1. Surface potential is at its lowest when there is no cavity, and it decreases when the dielectric constant is greater, if there is a cavity. For charged particles, the negatively charged biomolecules greatly shifted, within the nano-cavities, the surface potential to be much smaller than the neutral and positively charged circumstances, in which the positively charged analytes have the highest surface potential along the channel.

The researchers examined the impacts of neutral and charged analytes on the band diagrams of the device, in the following results.

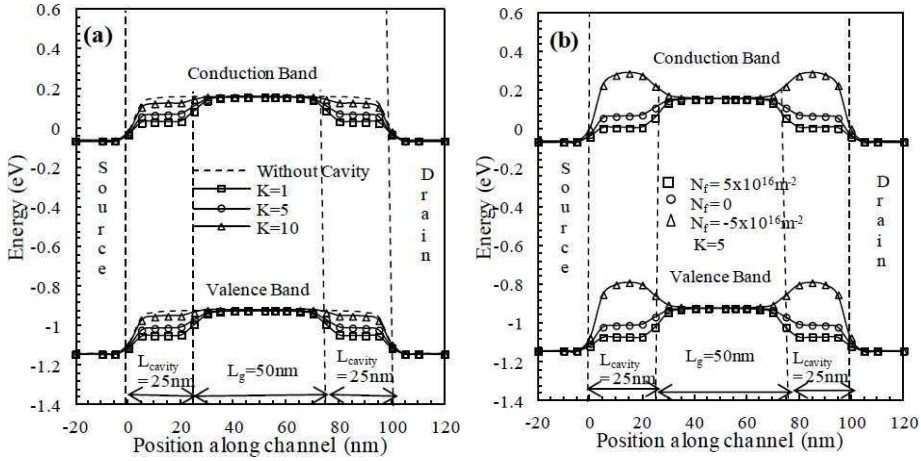

In the situation of neutrally charged analytes, without the cavity, the valence and conduction bands are at their peak energies in eV, and the lower the dielectric constant of the neutrally charged analyte, when and with the nano-cavity present, the lower the energy in eV, as it is shifted down compared to the lower dielectric constants or absence of the nano- gap examples. When observing the phenomena for the charged particles, the positive charged biomolecules in the cavity increase the energy, whereas the negative energy has it at the lowest. This phenomena is the inverse of the trend for the surface potential. The energy band is dependent on the change in flat band voltage within the cavity regions, which is also predicated on the nanogap cavity regions' capacitance and dielectric constant.

The researchers simulated the electric field for the device with respect to varying dielectric constants and biomolecular charges.

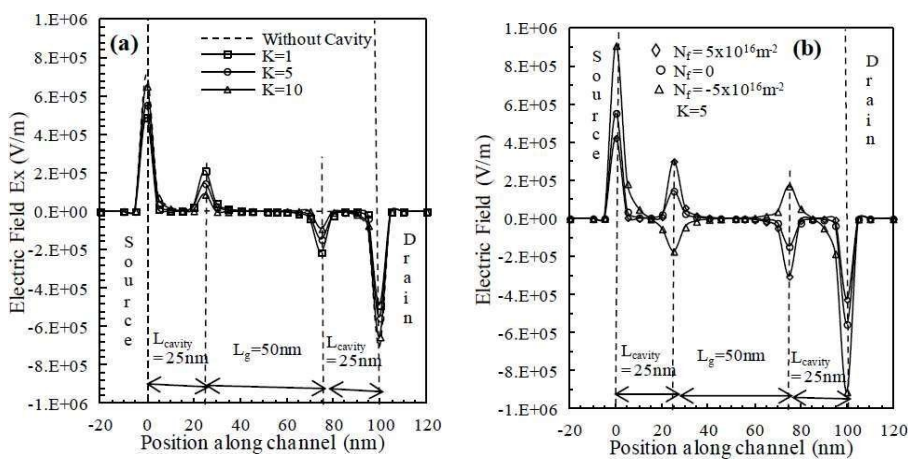

The peak electric field shares the same relationship as the previously mentioned energy graphs. The smaller peaks at the middle alternate, however. Before the cavity formation, there is no peak in the electric field over the channel region. With the influence of positively charged biomolecules, within the cavity regions, the electric field increases in magnitude, and the peaks are smaller with negatively charged biomolecules.

The next important factor that the researchers simulated were the transfer curve characteristics shown below.

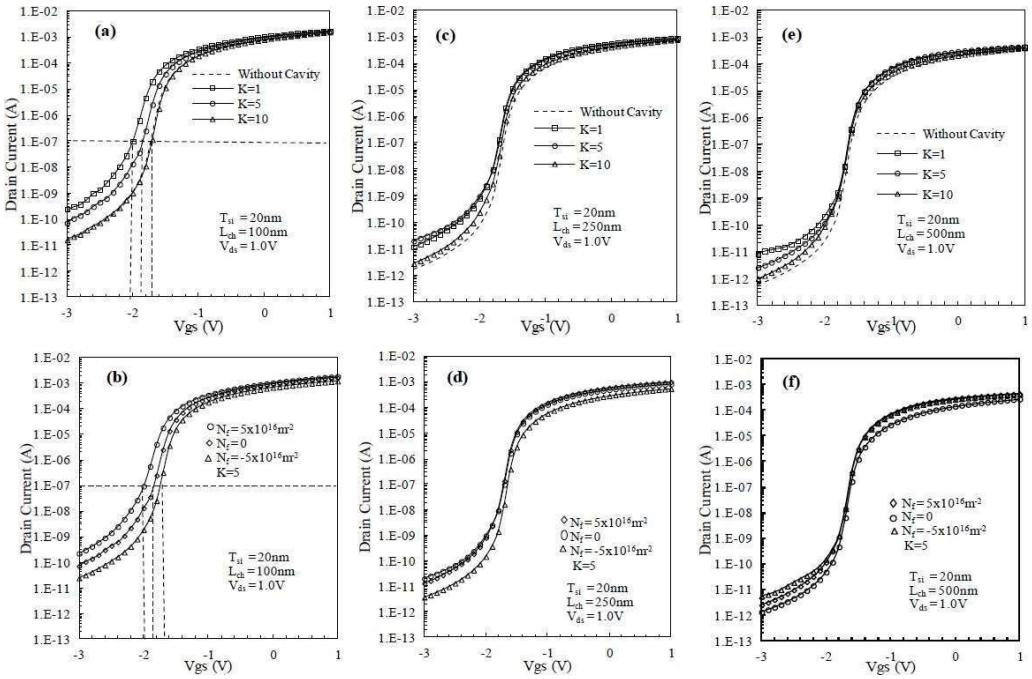

The observation indicates the influence of the channel length on the drain current carrying capacity, as a function of the dielectric constant for neutrally charged analytes within the nano-gap as the top row. In the bottom row, the influence of the analyte charge is taken into consideration along with the impacts on the growing channel length in the current carrying capacity. For larger dielectric constants, the biomolecules immobilized in the cavity help shift the threshold voltage when there was no cavity formation previously, this is indicated for in the bottom row. With positive charged analytes, the active current increases, whereas negatively charged analytes decrease the active current. For smaller devices, the impact of the threshold voltage is more substantial, such that channel length increases the off current at the expense of lower sensitivity.

The final parameter the researchers observed was the sensitivity as a function of the channel length and with varying dielectric constants and biomolecular charge profiles.

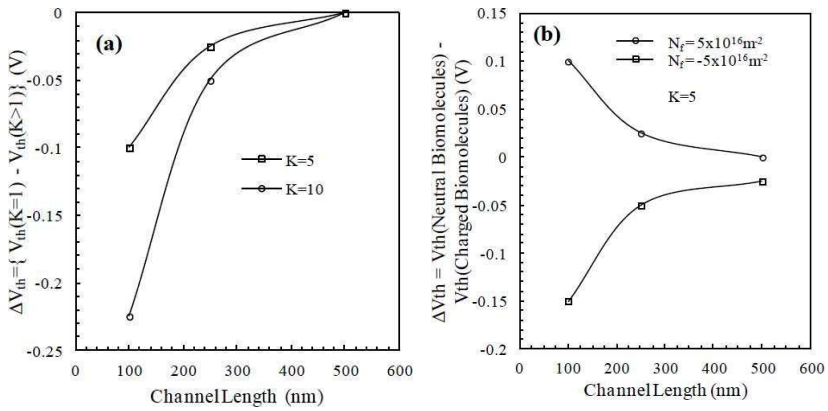

It is shown that the sensitivity saturates with increasing channel length, however, with shorter channel lengths, the lower dielectric constant has the advantage on sensitivity. This also applies somewhat to the positively charged analytes within the nano-cavity, which decreases in sensitivity with increasing channel lengths, however, it is still more advantageous over the negatively charged analytes, even at the channel length of 500 nm, despite the negatively charged analyte increasing in sensitivity with increasing channel length.

The researchers proposed the junctionless DG-DMFET as a biosensor, analytically modeling the surface potential, energy bands, electric field, sensitivities, and showing the impact of dielectric constants and biomolecular charge on all of these parameters for this device's design. Based on the research, for this design structure, shorter channel lengths are more advantageous in terms of sensitivity and also that negatively charged biomolecules have the largest impacts on the device's performance. The researchers concluded that n type devices are suitable for negatively charged biomolecule detection and p-type for positively charged biomolecule detection, in this device structure.

The next article to be discussed, per the literature review, is "A Novel Dielectric Modulated Gate-Stack Double-Gate Metal-Oxide-Semiconductor Field-Effect Transistor-Based Sensor for Detecting Biomolecules", conducted by researchers Dibyendu Chowdhury, Vishnu Prasad De, Bhargav Appasani, Navaneet Kumar Singh, Rajib Kar, Durbadal Mandal, Nicu Bizon, and Phatiphat Thounthong. In this research article,

performances are compared between the n-type junctionless DG-DMFET and the GS-DG-DMFET, where the Atlas device simulator is used for validation. Based on the research, the proposed GS-DG-DMFET has a higher active current to off current ratio, as well as having better sensitivity and suitability towards low power, high sensitivity, and high speed applications.

Gate stacking is indicated as being helpful for high-speed switching applications, in addition to being an excellent amplifier. The gate all around topology is determined to handle drain induced barrier loading better than the standard DG-DMFET topology, within the analytical modeling of a source referred to in the paper, which was conducted by Pati et al. in the paper “Study of body and oxide thickness variation on analog and RF performance of underlap DG-MOSFETs”. In addition, the paper mentions, in its introduction, ongoing research methods such as underlap double- gate MOSFETs, MOGA-based approaches, the use of high dielectric constant oxides, CRPSO, ALC-PSO, gate-engineered cylindrical MOSFETs, asymmetric DG-FETs, vertical dielectrically modulated tunnel FET-based biosensors, and the impacts of gate materials on the cavity.
The main focus of the paper’s scope is the comparison between the JL-DM-DG-MOSFET and the GS-DG-DMFET in terms of their performance benefits via analytical modeling.

The proposed model for the junctionless DG-DMFET is as follows:

Figure 1. Device structure of (**a**) n-type junctionless DM-DG-MOSFET; (**b**) n-type junctionless DG-MOSFET-based biosensor with cavity; (**c**) n-type junctionless DM-GSDG-MOSFET; (**d**) n-type junctionless DM-GSDG-MOSFET-based biosensor with cavity with channel length of 50 nm.

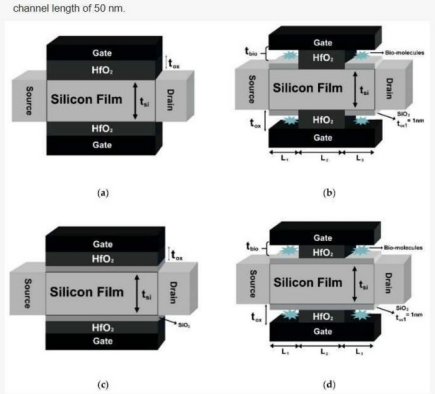

The proposed model for the junctionless dielectric-modulated gate-stacked double-gated MOSFET uses two oxide layers for the gate region, the oxide thicknesses are 1nm for the silicon dioxide and 9nm for the Hafnium dioxide. The procedure and proposed model is as follows:

Figure 2. The process flow of the n-type JL-DM-DG-MOSFET and JL-DM-GSDG-MOSFET (**a**–**l**).

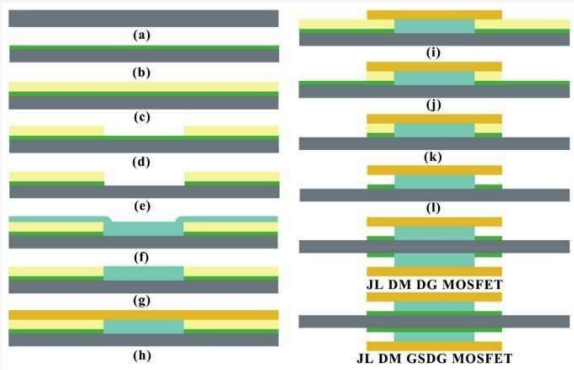

Next, the researchers used the Silvaco ATLAS simulator to analytically model and simulate the aforementioned biosensors, using neutral and charged biomolecules and variations in the dielectric constant variable. The output transfer characteristic curves are shown for the JL DM DG MOSFET vs the JL-DM-GSDG MOSFET to show the contrast of gate stacking on the performance.

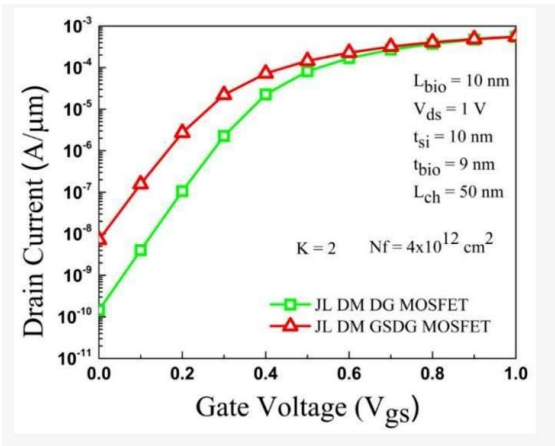

The general principles behind the device's operation are the biomolecule sensing regions are created at the drain and source sides as constructed nano-gap cavities, which, as previously discussed, are filled with biomolecules that impart dielectric changes impacting the electrical

characteristics. But furthermore, the capacitance modeling, which the researchers calculated, varies for these configurations than the previously noted designs. The researchers calculated the JL-DM-DG-MOSFET(left) and JL-DM-GSDG-MOSFET(right) effective capacitances as the following.

$$C_1 = C_3 = C_{eff}$$

$$C_{eff} = \frac{\varepsilon_{bio}\varepsilon_{ox1}}{\varepsilon_{bio}t_{ox1} + \varepsilon_{ox1}t_{bio}}$$

where ε_{ox1} is the dielectric constant of SiO_2.

$$C_2 = C_{ox}$$

$$C_{ox} = \frac{\varepsilon_{ox}}{t_{ox}}$$

where the dielectric constant of the gate oxide is denoted by $\varepsilon_{OX} = \varepsilon_2$.

For JL-DM-GSDG-MOSFET,

$$C_1 = C_3 = C_{eff}$$

$$C_2 = \frac{\varepsilon_{HfO_2}\varepsilon_{ox1}}{\varepsilon_{HfO_2}t_{ox1} + \varepsilon_{ox1}t_{HfO_2}}$$

where $t_{HfO_2} = (t_{ox} - t_{ox1})$ and $\varepsilon_{HfO_2} = \varepsilon_2$.

It is from these parameters that it becomes noticeable the influence of the double-stacked oxide inclusion into the general capacitance factor. The researchers also analytically modeled and simulated the electric field, surface potential, energy band diagram, and drain current characteristics, which are as follows.

Figure 5. Variation in electric field along the channel: (**a**) effect of K on JL-DM-DG-MOSFET; (**b**) effect of charged biomolecules on JL-DM-DG-MOSFET; (**c**) effect of K on JL-DM-GSDG-MOSFET; (**d**) effect of charged biomolecules on JL-DM-GSDG-MOSFET.

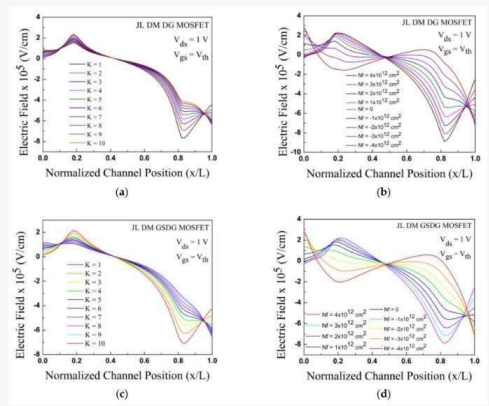

Figure 6. Variation in surface potential along the channel; (**a**) effect of K on JL-DM-DG-MOSFET; (**b**) effect of charged biomolecules on JL-DM-DG-MOSFET; (**c**) effect of K on JL-DM-GSDG-MOSFET; (**d**) effect of charged biomolecules on JL-DM-GSDG-MOSFET.

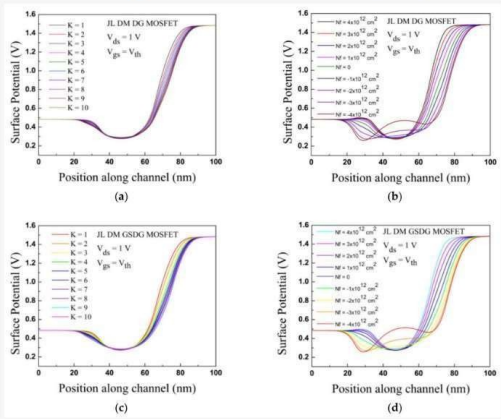

Figure 7. Plot of the energy band diagram for JL-DM-DG-MOSFET and JL-DM-GSDG-MOSFET at $V_{gs} = V_{th}$: (**a**,**c**) neutral biomolecules; (**b**,**d**) charged biomolecules.

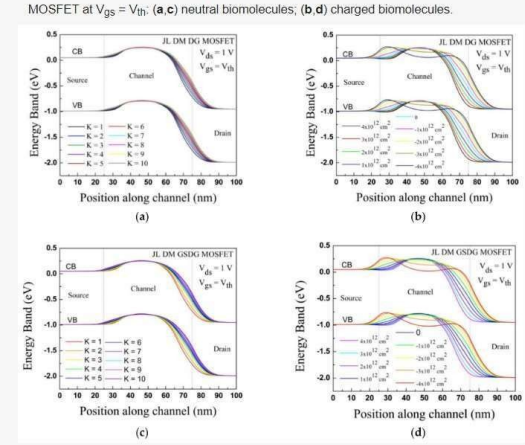

Figure 8. Plot of the transfer characteristics with V_{gs} for JL-DM-DG-MOSFET and JL-DM-GSDG-MOSFET: (**a**,**c**) neutral biomolecules; (**b**,**d**) charged biomolecules.

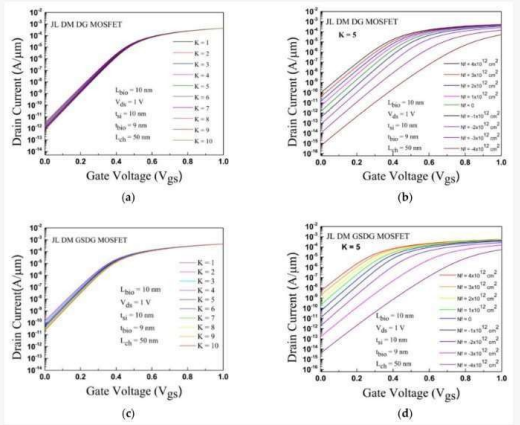

The peak electric field was investigated to be at K=1 within the source cavity, whereas the lowest electric field for K=1 was within the drain cavity. In the research finding, the electric field at the drain side is reduced for neutral and charged biomolecules, and electric field deformation occurs in the cavity regions. As per the surface potential factor, deformation happens underneath the cavity regions, and when cavities form, there is no reported deformation. Surface potential change at the source or drain-channel junctions is linear. Variations in the dielectric constant result in potential changes at the source and drain terminals, and, with positively charged biomolecules, potential increases slightly, whereas negatively charged biomolecules procure relatively sharp decreases in potential. This similar behavior was observed in the previous paper. As per the effect of gate stacking, the potential differences or larger at the source and drain terminals, and the potential profiled in the cavity regions depend on the dielectric constant. As per the energy band diagrams, cavity formations at gate oxides introduce the energy band profiles in which there is a downward trend towards the drain region being exhibited in junctionless device behavior. This behavior indicates easy carrier injection from the source to the drain. And lastly, for the drain current simulations, the dielectric constant of neutral biomolecules impacted the transfer curve characteristics, and the active and off currents decrease with the increase of the dielectric constant. In regards to biomolecular charge, active and off currents decrease with a negative charge profile, and increase with a positive charge profile.

The next important factor that the researchers looked at were the threshold voltages and sensitivity factors.

Figure 10. Variation of threshold voltage for JL-DM-DG-MOSFET and JL-DM-GSDG-MOSFET: (**a**) neutral biomolecules; (**b**) charged biomolecules.

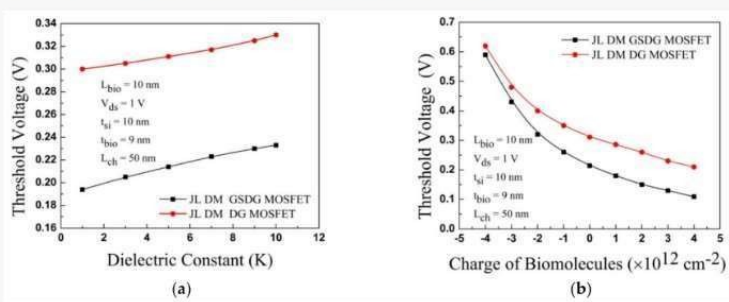

The research indicates that, for neutral biomolecules, the junctionless DM-DG MOSFET has larger threshold voltages at dielectric constants varied from 1 to 10. In addition, the JL-DM-DG MOSFET has a slightly larger threshold voltage for negatively charged biomolecules, where the difference becomes larger as the charge tends towards positive charges or neutrality.

The researchers analytically modeled the change in threshold voltage or sensitivity factor of both topologies and a 100 nm channel length device structure, observing the impact of dielectric constant and biomolecular charge on this factor.

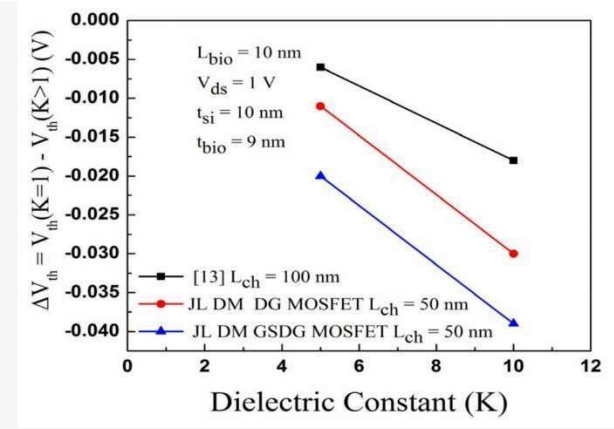

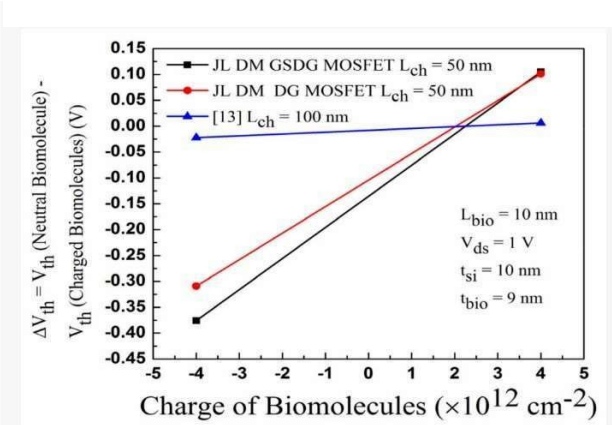

From the analytical modeling, for neutral biomolecules, at all available dielectric constants measured, the JL DG-DM-MOSFET has closer to 0 sensitivity than the gate stacked counterpart. This roughly applies for charged biomolecules, until the charge of the biomolecule is near 4E+12, in which the sensitivity performance is roughly tantamount. However, in practically all conditions, the DG-GS-DM MOSFET, from the analytical modeling, has outperformed the gate stacked counterpart in sensitivity performances, as it has higher sensitivity in absolute value terms for most of the range.

The researchers also examined the active to off current ratio, finding that, via the analytical model, the gate stacked design outperformed the JL DG-DMFET when it comes to charged biomolecules as well as most neutral biomolecules until very high dielectric constants such as k = 10.

Figure 13. Plot of the I_{on}/I_{off} ratio for JL-DM-GSDG-MOSFET and [13]: (**a**) neutral biomolecules; (**b**) charged biomolecules. Plot of the I_{on}/I_{off} ratio for the JL-DM-GSDG-MOSFET and JL-DM-GSDG-MOSFET: (**c**) neutral biomolecules; (**d**) for charged biomolecules.

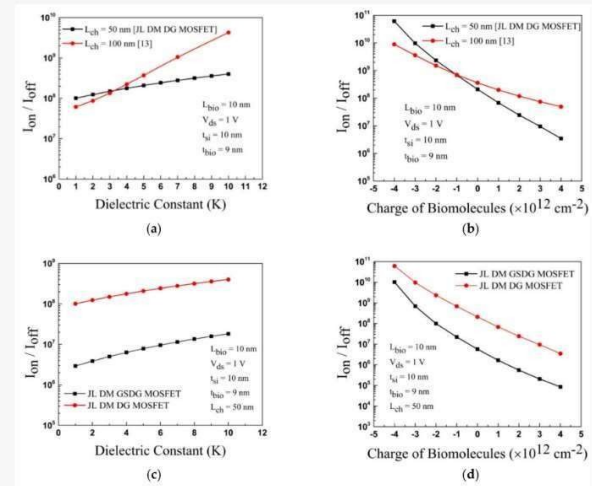

Figure 14. (**a**) Threshold voltage sensitivity of JL-DM-DG-MOSFET, JL-DM-GSDG-MOSFET, and reference [13]; (**b**) sensitivity improvement in JL-DM-DG-MOSFET and JL-DM-GSDG-MOSFET over [13].

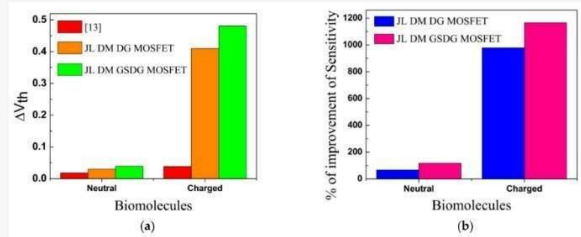

The researchers also looked at the impact of gate stacking on the RF performance and noise characteristics.

Figure 15. Plot of (**a**) g_m, (**b**) g_m/I_{ds}, (**c**) $C_{gs} + C_{ds}$, (**d**) f_T, and (**e**) GBP with gate voltage for JL-DM-DG-MOSFET and JL-DM-GSDG-MOSFET biosensor at K = 5.

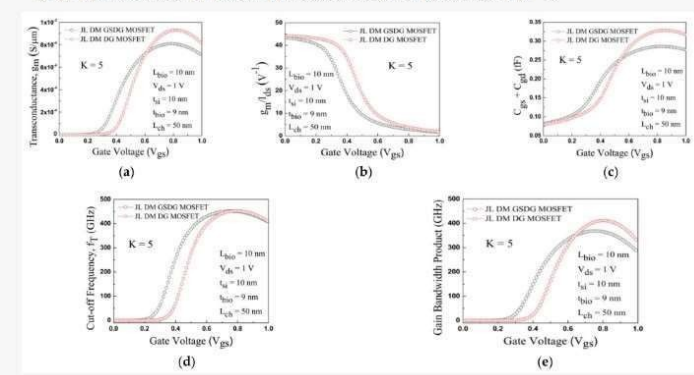

Figure 16. Variation in (**a**) *gm3*, (**b**) V_{IP3}, (**c**) IIP_3, and (**d**) IMD_3 with gate voltage for JL-DM-DG-MOSFET and JL-DM-GSDG-MOSFET biosensor at K = 5.

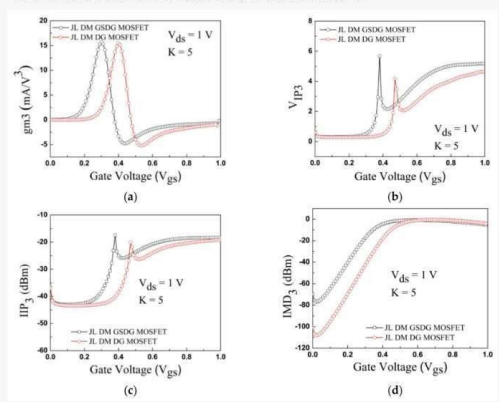

Based on the research, a higher transconductance is favorable for carrier transport efficiency, and the transconductance to channel current is a metric for whether the device exhibits low power dissipation at the capacitive load. The gate-source capacitance and gate-drain capacitance sum will be an indication of the gate voltage, where the Cgg refers to the subthreshold region and how driving the gate will impact the low inversion charge. In addition, cut off frequencies are displayed, in which both device configurations exhibit high cut-off frequencies at high gate voltages which is

advantageous in RF design. Additionally, the research has shown the gain-bandwidth product to fall with higher gate voltages, indicating that these biosensors are better suited for low-power applications. As per the noise characteristics, the peak gm3 is nearly the same, with improvements on the signal-to-noise ratio near the DC bias point. The research indicates that gate stacking is less affected by noise, considering the Vip3 peak reflects the cancellation of the third order nonlinear effects from phenomena such as internal feedback and second order effects. The gate stacked design offers a better IIP3 at lower gate voltages, which is better suited for this application. Additionally, and finally with regard to noise characteristics, the analytical model shows a smaller IMD3 point in the gate stacked configuration, which is a better indication of less noise impact.

To conclude the team's research findings, the gate stacked configuration is better suited, in terms of sensing performance, for neutral and charged biomolecules, as it sees higher improvement. In addition, gate stacking has boosted the active to off current ratio relative to the design topology without gate stacking. It is also concluded that the JL DM GS-DG DMFET has a smaller threshold voltage and is more immune to noise than the non-gate stacked device, where both are suited for a low-power application.

The next article which will be discussed, in this literature review, is "Gate Engineering on the Analog Performance of DM-DG MOSFETs with High K Dielectrics", conducted by researcher Nirmali, Vijaya Kumar. In this research paper, an investigation of gate engineering's influence on RF and analog performance with high k dielectrics is observed via a 2D device simulator. The specific technology employed is the dual metal gate technology, which has benefits in drain induced barrier loading immunity as well as improved analog performance with regards to transconductance, output resistance, and early voltage.

The issue discussed, in this paper, among sub 0.1 micron regime devices, is the short channel effects and higher gate leakage, which necessitates gate engineering approaches to solving these issues. The DG-DMFET is noted as an excellent option, based on its immunity to short channel effects

and immunity to high leakage currents. In addition, it provides better gate control and has emerged as a promising technology for its sensitivity and other performance benefits. One other example is the very light doping reducing mobility degradation as well as the second gate reducing drain induced barrier loading as well as providing additional gate control. The researchers note the uses of gate engineering proposed as two gates with different work functions merged together to form a single gate of a bulk MOSFET. In the gate engineering, some designs propose the gate material to be closer to the source terminal end, to improve the electric field and electron velocity along the channel, thereby improving the gate transport efficiency. In this proposed configuration if drain voltage exceeds drain saturation voltage, excess voltage is then absorbed by the gte metal which prevents the drain field from penetrating the channel. In addition, the step potential lowers subthreshold leakage current, thereby mitigating DIBL effects and increasing the output resistance. This example of gate engineering allows for the device to maintain its threshold voltage with reduced doping concentration in the channel, mitigating mobility degradation which improves the transconductance, useful in RF and analog applications. Due to the down-scaling of transistors silicon dioxide dielectrics have decreased more steadily, and in accordance with improving gate capacitance, drive current, and other device performance factors. However, this downscaling also presents an increased risk of quantum tunneling and leakage current. This is why a high K material is proposed, as it will increase the gate's capacitance, an intended effect, without the leakage issue.

The researchers propose the following dual-gated MOSFET structure:

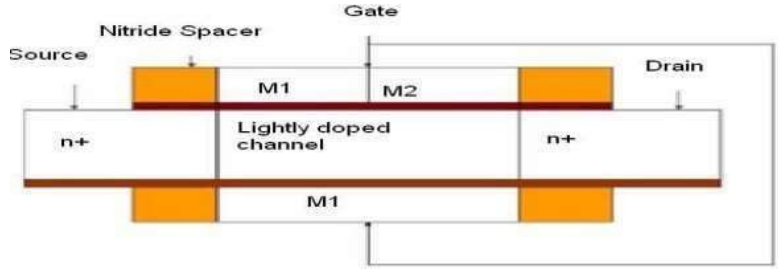

The results are then generated via the process simulator DIOS and its device simulator DESSIS which regards the integrated systems engineering technology computer aided design. A wide range of dielectric constants are used in this analytical modeling, including a dielectric constant as high as 40.

To verify the analog performance parameters, the transconductance generation factor is observed, which refers to the transconductance to drain current, and is a good metric for power dissipation as well. The maximum point of this parameter during weak inversion, and it degrades with increasing drain current when the device is in strong inversion. The following figure is the simulated result of the proposed model.

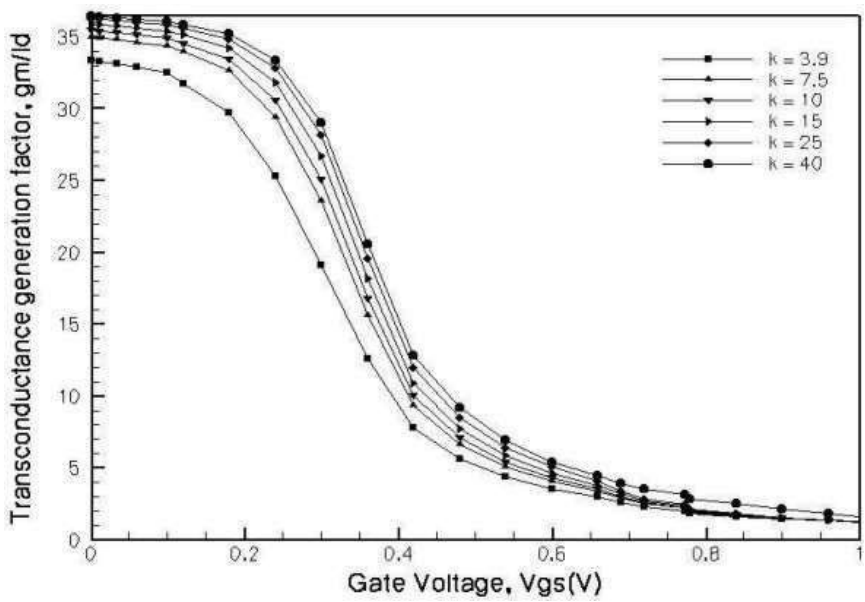

Increasing the dielectric constant imparts a better characteristic of the transconductance generation factor.

In the next simulation, the researchers observe the transfer curve characteristics, Id vs the Vds, with varying dielectric constants, indicating that smaller dielectric constants have larger currents.

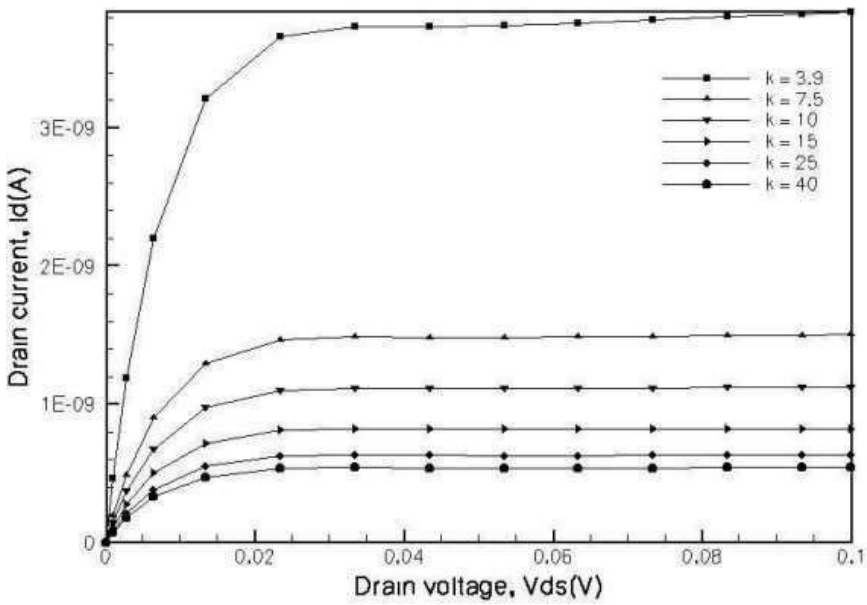

Since the drain currents are evaluated with respect to the drain voltage and dielectric constant, the researchers then use these variables to analytically model the output resistance as a function of the dielectric constant, where the output resistance is referring to the early voltage divided by the drain current. The following is the analytical model's simulation results of this output resistance factor. The trend is that dielectric constant values are directly proportional to the output resistance, with the largest output resistance occurring when the dielectric constant is 40.

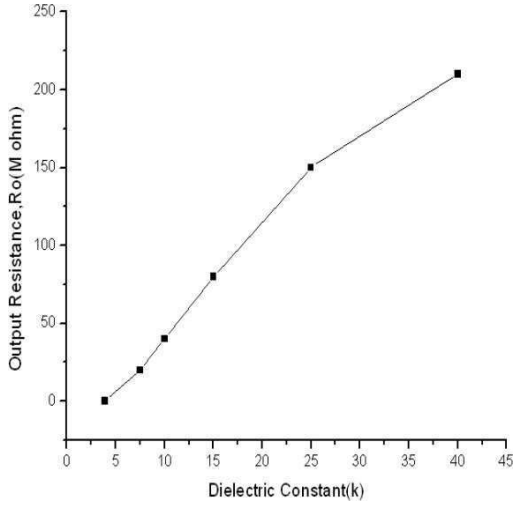

The early voltage is also simulated as a function of the dielectric constant, and has a similar pattern and relationship, as it would be expected.

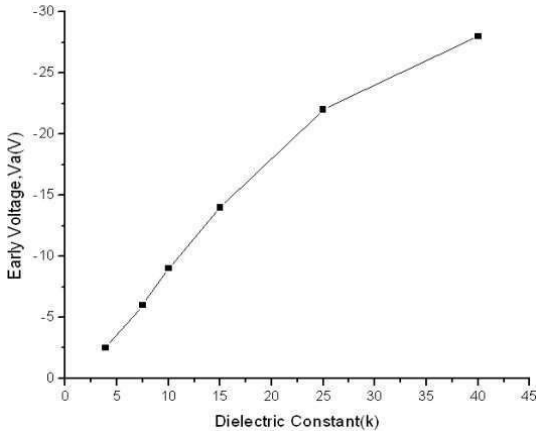

To conclude, the paper analyzes the impact of gate engineering on analog performance factors for the DM-DG MOSFET design structure. The relationship is shown between early voltage, output resistance, drain current, transconductance, as functions of the dielectric constant, thereby showing the performance benefits with using a high k dielectric oxide layer for this gate-engineered DM-DG MOSFET design. The researcher notes that this technology is most favorable in low-power and subthreshold analog applications, where the improvement is especially present within the weak inversion regime of the device, hence its more desirable performance outcomes in the low-power subthreshold conditioning.

The next research paper, discussed as a part of this literature review, is “A Device Simulation based Investigation on Dielectrically Modulated Fringing Field Effect Transistor for Biosensing Applications”, conducted by researchers Sayan Kanungo, Sanatan Chattopadhyay, Kunal Sinha, Partha Sarathi Gupta, and Hafizur Rahaman. In this research paper, a dielectrically modulated fringing field effect transistor is proposed as a transducer element for electrochemical biosensing, in which the gate- induced fringing field is used in the transduction. The researchers discuss that this differentiates from the DMFET-based transducers, and the researchers compare this structure to the DMFET and DG-DMFET based structures.

The researchers discuss two approaches in the performance boosting aspects of these classifications of bio-sensors– bio-receptor optimization and transducer optimization. Different device structures have been proposed, throughout the years, to influence direct gate field modulation from bio-molecule conjugation. This research paper is purported to be the first instance of the DMFFET structure proposed, in which the biomolecule detection is done via the gate-induced fringing field. This method is different from the typical DMFET approach, in which the fringing field is insignificant to the device operation.

The researchers proposed the following device structures, and modeled by Synopsys Sentaurus TCAD, which the researchers note as a simplified representation of a practical situation.

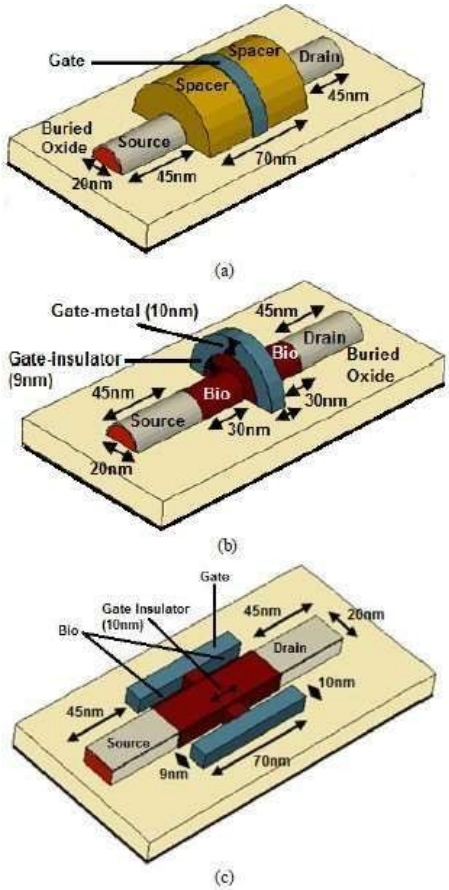

Schematics of: (a) FFET, (b) DMFFET transducer, (c) DG-DMFET transducer. Dimensions in this figure are not in scale.

The fringing field controlled electron injection over the source/ channel junction determines the general conduction of the field-fringing effect based device structures. The researchers also note that gate induced fringing field modulation has been thoroughly investigated, and that, for any bias on the gate or drain terminals, the polarization electric field exposes channel regions in which the electrostatic conditions are determined. Higher polarization field mitigates the fringing field strength, whereas lower polarization field increases the fringing field strength.

Within the scope of the researchers' paper, an investigation is made looking into the carrier transport and electrostatic mechanisms at the gates of the field-fringing effect transistor and its dielectrically modulated adaptation. The researchers analytically modeled the effects on carrier transport mechanisms via the lateral electron current density. From this simulation result, a higher polarization field within the spacer region reduces the region's potential drop, thereby reducing the channel's surface potential and greatly hindering current density.

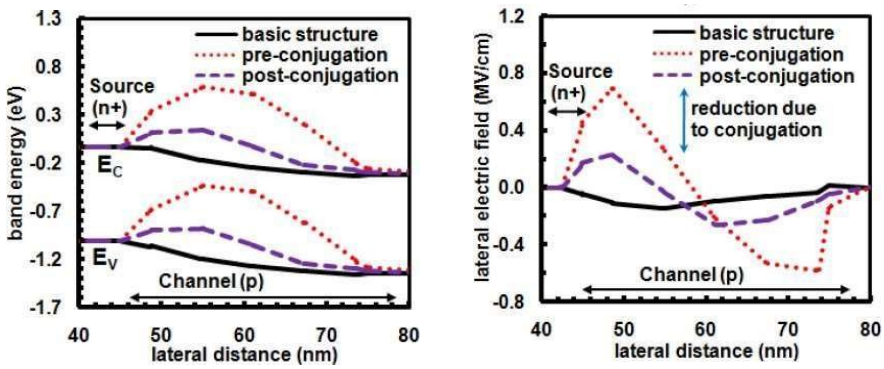

The drift field, depending on the maximum lateral electric field, opposes the electron diffusion flux into the channel. With greater coupling between the gate and the channel, the drift field would be reduced substantially. It is remarked, by the researchers, that, for the FFET, the field is extremely low or even opposite direction-wise, which means that the flux from source into the channel is very high. As for the DMFFET, the drift field is enhanced, as a result of spacer elimination, causing the junction to be reverse biased,

and thereby degrading drain current and flux. The researchers also noted that the flux is improved with conjugation or binding/creation of the analyte- receptor complex.

The researchers investigated the relative efficiency of the fringing field transduction mechanism, creating simulated profiles below.

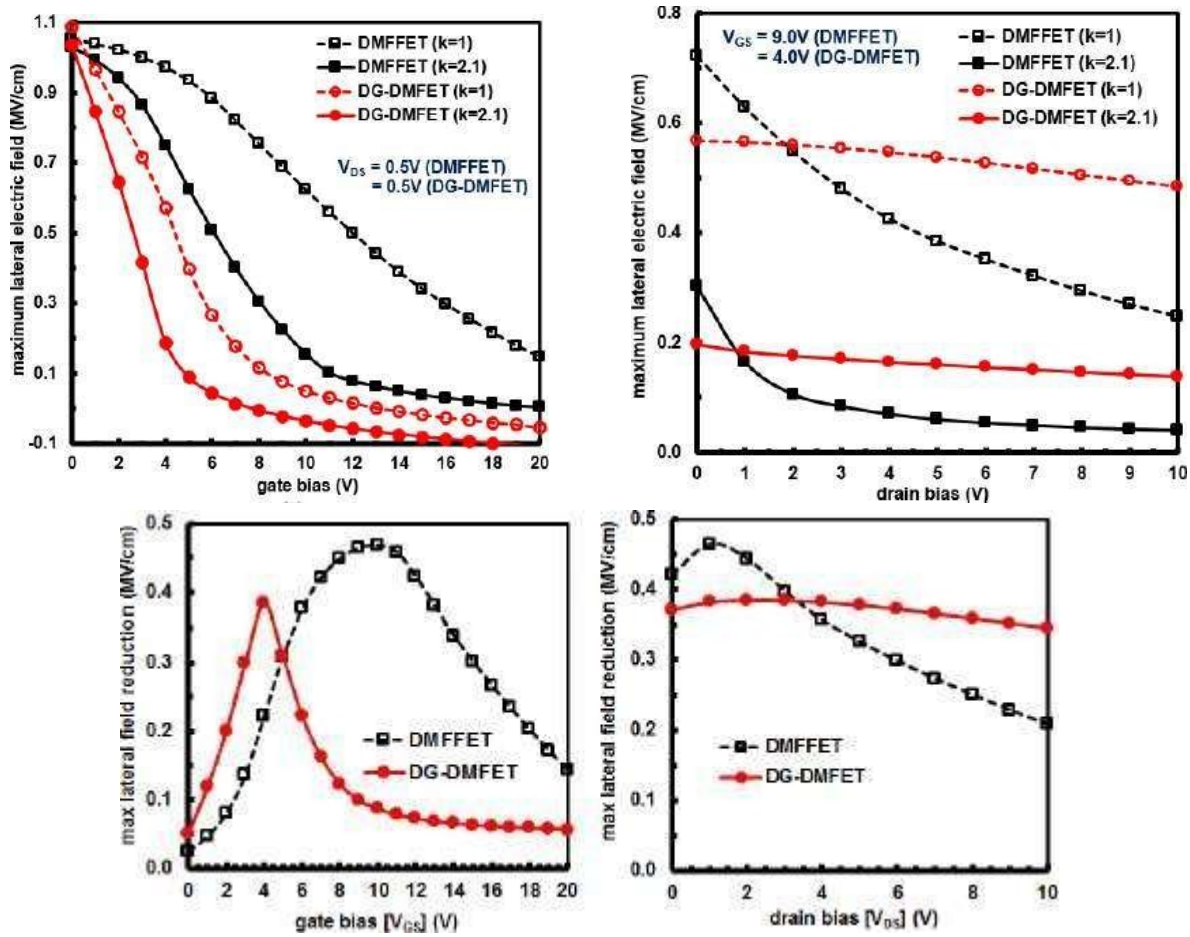

As the researchers commented, the conjugation induced gating effect modulation is a key mechanism for all dielectric modulated FETs, upon which the electrostatic influence of the gate is important in that it enhances the electric field within the nano-gap and exposed channel, improving electrostatic modulation and further gate bias increases channel inversion which restricts electrostatic modulation of analyte-receptor binding.

Based on the research, a smaller channel inversion at a sufficiently high gate bias is beneficial to transduction, and which can be ensured via low

gate-to-channel coupling which induces the fringing field effect. Once the gate bias increases in this scenario, the drift field is much greater than the DG-DMFET design.

The researchers analyze the optimum transducer response as the half- width at full maxima operating point in which the drain current sensitivity is greater than or equal to half of its maximum. The drain current sensitivity is mathematically defined as 20 times the logarithmic ratio of drain current with biomolecular activity in the nano-gap to drain current without this activity.

The researchers then obtain transfer and output curve characteristics,
for the DMFFETs and DG-DMFETs, with two possible dielectric constant values, as well as drain current sensitivities as functions of gate bias and drain bias.

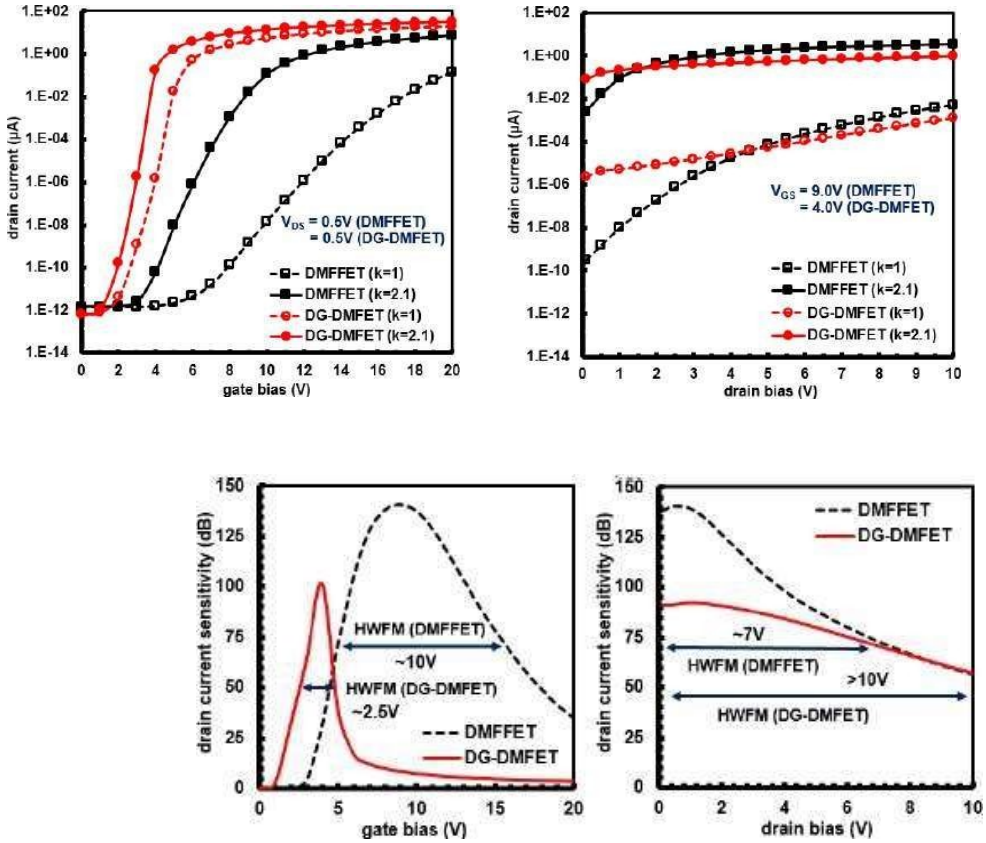

The DG-DMFETs have higher current carrying capacities, per smaller gate biases, indicating ease in gate control. However, the DMFFET has higher

drain current sensitivities as functions of gate bias at higher voltages, meaning that, if power consumption is not too concerning, it has better performance, however, the DG-DMFET performs better in low-power applications. The DMFFET has higher drain current sensitivity with respect to drain biasing.

The next factor considered by the research team is the sensitivity differences and differences between threshold voltages per these two device configurations. For the typical DMFET, it is advantageous to have a larger threshold voltage, as an improvement on the sensitivity. The researchers commented that trapping and detrapping an electron is equivalent to gating effect perturbation, where weaker gate bias dependence of sensitivity in the DMFFET causes smaller sensitivity variations.

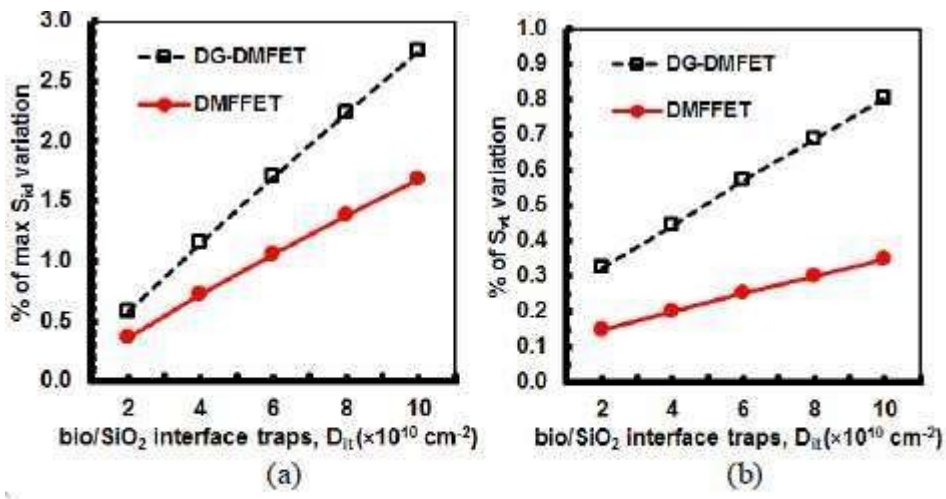

Comparative plots of variation in: (a) maximum drain current sensitivity, (b) threshold voltage sensitivity, at different bio-molecule/gate-insulator interface trap-state density for DMFFET and DG-DMFET.

In this analytical model, the advantage of the DG-DMFET in drain current sensitivity and threshold voltage sensitivity has been shown, via analytical model simulations. The DMFFET is dependent on gate control and the gate-induced fringing field for its sensitivity performance. For the optimal sensitivity, in this case, the fringing field must be high with less direct gate control. In order to improve upon this factor, what is proposed is a different

gate insulator material and thickness, including adjustments to the gate-to-channel ratio. A lower dielectric oxide or insulator reduces the gate control, heightening the fringing field effect, whereas a thicker gate insulator increases the fringing field but reduces gate control. It is concluded then that a thick low-dielectric insulator is optimal for improving the sensitivity for this application. The researchers also comment that reducing the gate- to-channel ratio has the observed effect of increasing the fringing field magnitude and reducing gate control. The researchers simulated and modeled the impact of gate insulator materials and their respective thicknesses on the drain current sensitivity as well as gate-to-channel ratios' impacts on drain current sensitivity.

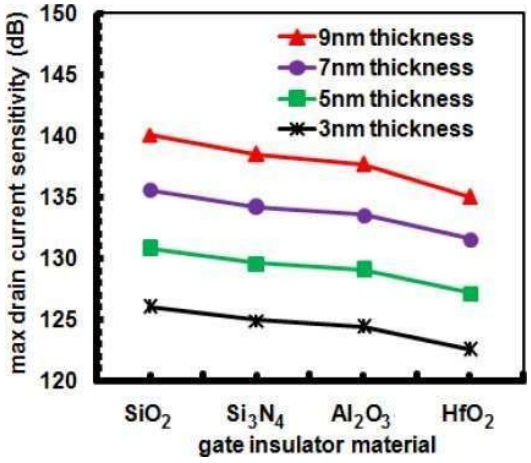

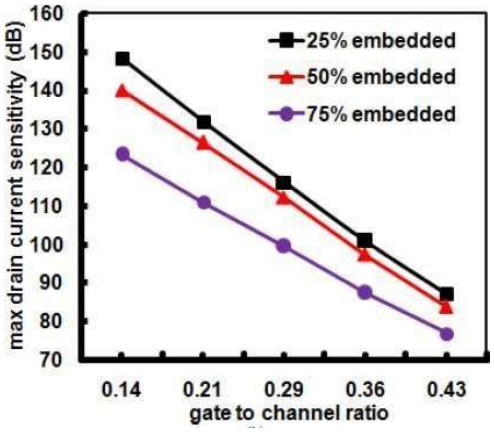

As previously mentioned, gate thickness corresponds with increases in the drain current sensitivity. In addition, smaller gate-to-channel ratios have higher drain current sensitivities correspondingly as well.

The next comparative analysis the researchers make is on the transduction efficiency, which is predicated on maximum drain current sensitivity and threshold voltage sensitivity, as it varies for different biomolecular charge profiles.

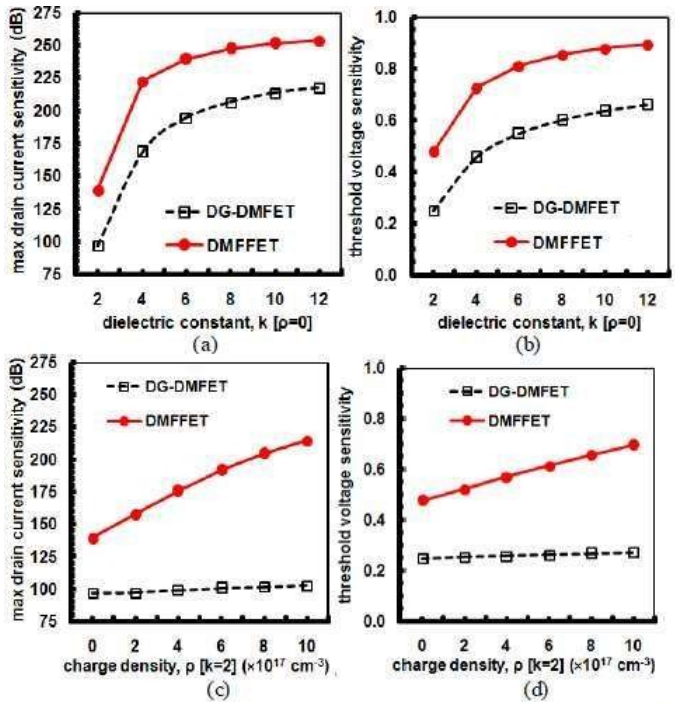

Comparative plots of: (a) maximum drain current sensitivity, (b) threshold voltage sensitivity for different bio-molecule dielectric constant, and on: (c) maximum drain current sensitivity, (d) threshold voltage sensitivity for different bio-molecule charge density, for DMFFET and DG-DMFET.

The results indicated in this analytical model show the superior drain current and threshold voltage sensitivities of the field-fringing effect device structures which were augmented on the fringing field magnitude front. Increasing dielectric constant biomolecules influence the electrostatics at lower gate biases. This results in an increased performance benefit, with regards to the field fringing effect designs, however, with the DMFFET, there is weaker gate-to-channel coupling in which the comparative sensing efficiency of the DMFFET reduces. The impact of positive charge densities on the electrostatic effect of conjugation is more prominent in the DMFFET as well, because of the larger surface-to-volume ratio.

To conclude, in this research paper, the DMFFET design has been analytically modeled on its performance and transfer curve characteristics and compared to the DG-DMFET design. Based on the research, shorter and thicker gate-stack formations cause the direct gate field to not be able to control the gate induced fringing field which is used for transduction and as a part of the bio-sensing mechanism. The lesser gate-to-channel

coupling of the fringing field with the junction indicates higher sensitivity and a wide bio-sensing range, however, the trade-off is that this not as strong coupling makes it so the DMFFET is not sensitive towards electron trapping and detrapping, relative to the DG-DMFET design. The biasing plays an especially important factor in determining transduction efficiency and the DMFFET operating range, which is also influenced by gate- insulator material composition/thickness, gate-to-channel ratio and cylinder- embedding percentage of the transducer which also greatly influence the DMFFET parameters.

The next research paper, discussed as a part of this literature review, is “Simulation of Field-Effect Biosensors (BioFETs)”, conducted by researchers Thomas Windbacher, V. Sverdlov, Siegfried Selberrherr, Clemens Heitzinger, Norbert Mauser, and Christian A. Ringhofer. This research paper concerns the modeling of BioFETs and the influence of charged atoms and the dipole moment and surface density calculations. In this research paper, the capability of a BioFET is shown in its detection of specific DNA and the resolution of its orientation.

The research paper notes the current technologies in pathogen detection such as tumor markers, antigen-antibody complexes, and their limitations such as cost and time consumption. The process noted for detection of specific DNA involves several steps noted in the literature. The sequence of these steps is amplification of the biomolecule concentrate via PCR with labeling, then the solute biomolecules via a microarray, then the cells are are read via laser beams and a microarray, and the process is considered more time extensive and expensive in cost compared to the advantage brought by BioFETs. One advantage noted in the literature is that BioFET can sense the biomolecules without the use of PCR, which means additional equipment such as optical readers and microarrays are not needed. The researchers utilize a homogenized interface model as a structured BioFET description, and the DNA hybridization reaction is modeled.

The researchers provide a generalized structure of the BioFET, detailing the solute, reference electrode, and analytes and receptors within the aqueous solution. The figure that is proposed is as follows.

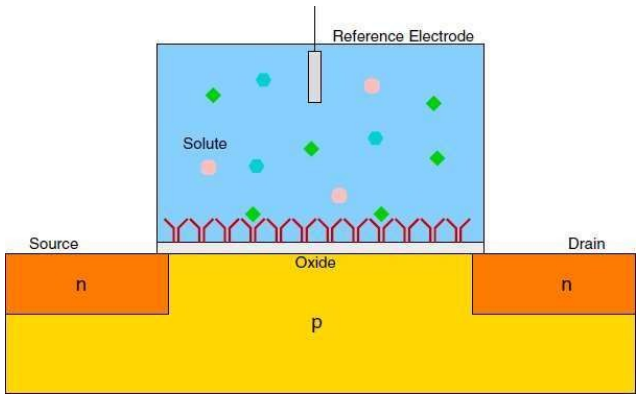

The researchers note that for DNA hybridization, salt is required, as it reduces repulsive forces between the DNA strands, thereby speeding up hybridization with the trade-off of less signal due to stronger screening. The researchers solved the Poisson-Boltzmann equation of the solute with the sodium chloride factored in. kB is boltzmann's constant, T is temperature, sigma = +/- 1 for a salt, epsilon refers to vacuum permittivity, ψμ is chemical potential, (c_sigma)∞ refers to ion concentration at equilibrium, epsilon_Ana is the water permittivity, all variables which denote the carrier densities derived of the Boltzmann model.

$$\epsilon_0 \nabla \cdot (\epsilon_{Ana} \nabla \psi(x,y)) = -\sum_{\sigma=\pm 1} \sigma \; q \; c_\sigma^\infty \; e^{-\sigma \frac{q}{k_B T}(\psi(x,y)-\psi_\mu)}$$

The researchers model the surface change due to chemical reactions as a response to the analyte. Ns refers to the surface binding site density, whereas Ka and Kb are equilibrium constants of the positive surface and negative surface charges respectively. The [H+]b refers to the bulk's

hydrogen ion concentration . The researchers detail varying surface binding site densities for different material compositions

$$Q_{Ox} = q\ N_S\ \frac{\frac{[H^+]_b}{K_a}\ e^{-\frac{q}{k_B T}\Psi(x,y)} - \frac{K_b}{[H^+]_b}\ e^{\frac{q}{k_B T}\Psi(x,y)}}{1 + \frac{[H^+]_b}{K_a}\ e^{-\frac{q}{k_B T}\Psi(x,y)} - \frac{K_b}{[H^+]_b}\ e^{\frac{q}{k_B T}\Psi(x,y)}}.$$

Oxide	pK_a	pK_b	$N_S\ [cm^{-2}]$
SiO_2	-2	6	5.10^{14}
Al_2O_3	6	10	8.10^{14}
Ta_2O_5	2	4	10.10^{14}
Gold surface	4.5	4.5	1.10^{8}

The researchers note that charged molecules binding to the receptors change the potential near the transducer-surface, influencing the field- effect and conductance within the channel of the transistor at the Angstrom scale whereas device dimensions are in the micro or potentially nano scale depending on the FET design. The researchers discuss the importance in modeling the transducer-solution interface, and the impacts of biomolecule charges and charge distribution, which, with the influence of the charge and dipole moment of single molecules from protein data banks, influences the surface density as well as the electrical parameters of the device’s performance.

An equation is referred to, as a description of the field changes from surface charges at the interface, where the following equation refers to the dipole moment’s purported potential shift which considers the analyte’s potential adjustment. The researchers ran simulations to model two surface concentrations of bound DNA, in which mean distance and potential profiles at varying states were derived out of the states in which there was an unprepared surface with no DNA attached, a prepared unbound state with single-stranded DNA bound, and a bound state with single-stranded DNA hybridized to double stranded DNA. The orientations were also considered in this study, in which the positions were surface perpendicular and surface parallel, and 100% binding efficiency was assumed in this

analytical model for the optimal characteristics and outer bound conditions of practical application.

The researchers ran simulations to find the potential profile of the BioFET with the inclusion of the solute, in which it is observed that negatively charged DNA's attachment to the interface produces an increase in the potential shift and decrease in the threshold voltage, increasing the channel resistance.

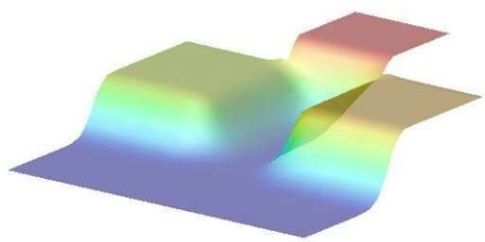

Potential profile for double-stranded DNA perpendicular to surface for the whole device.

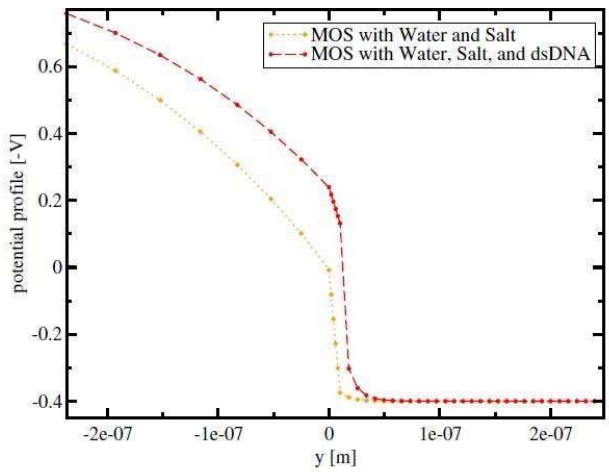

Potential profile at the interface (from left to right: semiconductor, oxide, solute).

From the simulations, the DNA surface concentration impacts the single- stranded DNA unbound state, DNA surface concentration impacts the double-stranded DNA bound state, and the output curves increase with higher concentrations and smaller channel length modulation. The research

concludes that the bound double-stranded DNA state has greater negative surface charge, due to a larger number of elementary charges (24 vs 12) and this purports a reduction in current, in which it becomes more significant with higher DNA concentrations.

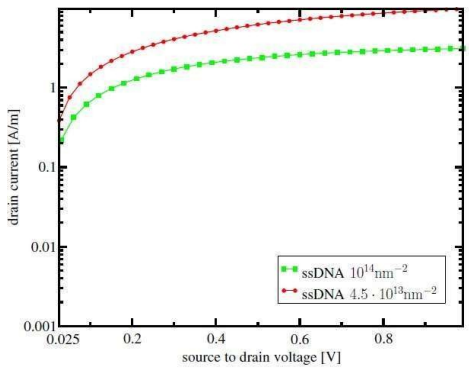

Output characteristics of MOS before hybridization, for mean distance $10^{14}\mathrm{nm}^{-2}$ and $4.5 \cdot 10^{13}\mathrm{nm}^{-2}$ without dipole moment.

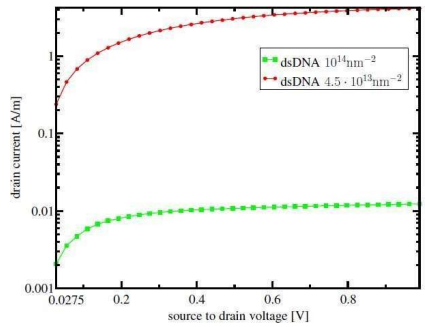

Output characteristics of MOS after hybridization, for mean distance $10^{14}\mathrm{nm}^{-2}$ and $4.5 \cdot 10^{13}\mathrm{nm}^{-2}$ without dipole moment.

As indicated, the impact of hybridization on the higher DNA concentration, 1E+14 (nm^-2) without the dipole moment is much more substantial, and this is due as well to the aforementioned phenomena of larger negative surface charge reducing the drain current.

The researchers derive the output curves based on DNA orientation, showing that when DNA is perpendicular to the surface, the resistance is at its highest. When the DNA is parallel to the surface, the resistance is greater than the curve lacking the dipole moment, because of the inhomogeneous charge distribution and its associated dipole moment that is linked. The researchers analytically modeled the respective potential profiles to these differences in DNA orientation, in which the perpendicular state corresponds to the most negative shift in threshold voltage, and in which the parallel state corresponds to an almost negligible effect compared to the dipole moment situation. It is noted that biomolecules are inhomogeneously charged, thereby purporting a dipole moment in which the orientation is configured such that energy is minimized.

The researchers note that optical detection is valuable in deciding the linking molecule to mitigate or remove the possibility of steric hindrance, receptors blocking accessibility to other receptors, and situations in which

binding sites are blocked. It is noted that a short linker, which is ideally neutrally charged or as close as possible to it, as the charge may be considered additional noise, may be advantageous in that it keeps distance from the surface minimized, improving the signal-to-noise ratio.

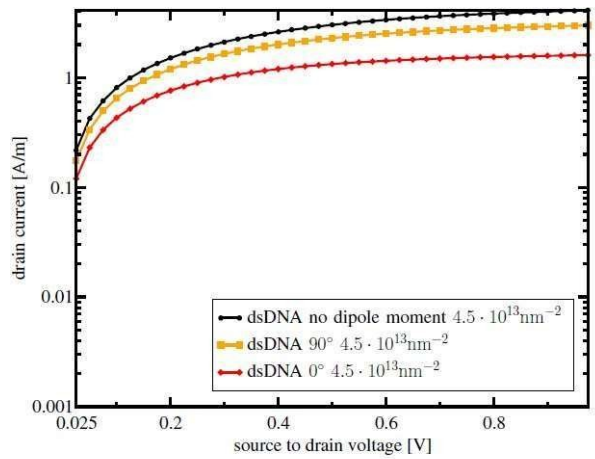

Output characteristics of MOS after hybridization, for mean distance $4.5 \cdot 10^{13}\mathrm{nm}^{-2}$: without dipole moment, with 0°, and 90°.

The double stranded DNA lacking the dipole moment has the largest drain current capacity, whereas the perpendicular orientation yields the smallest drain current and is the highest in channel resistance. The parallel orientation does not confer as great of a change, but it is slightly less conductive and more resistive than the double stranded without the dipole moment case.

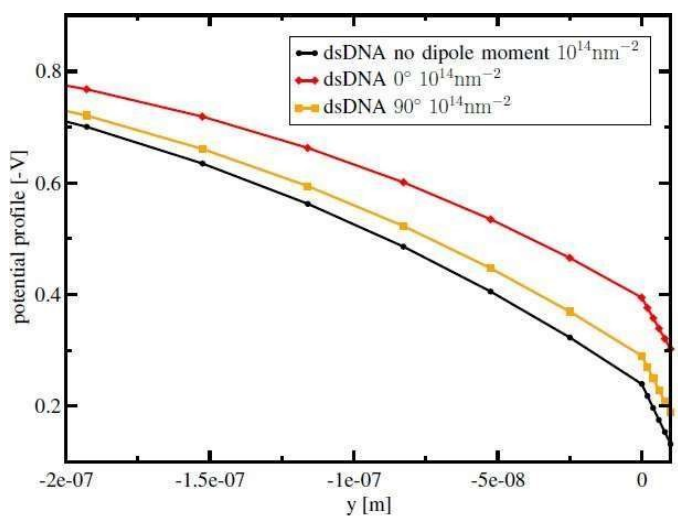

Potential profile from semiconductor to oxide (left to right).

To conclude the research article, the analytical modeling performed indicates that there is strong dependence on surface charges and that DNA hybridization is resolvable, and the impacts of hybridization and orientation on the electrical characteristics such as the potential profile, drain current, channel resistance, and threshold voltage are noted. This study factors in the biomechanics at the surface level of the BioFET and the respective changes which are documented from the analytical model, comparing orientations and other factors. This literature is important in describing the biological phenomena, such as the molecular mechanics at the surface and behaviors which impact the sensing and device's performances.

The next and last article reviewed for the literature review is "Electrical nanogap devices for biosensing", conducted by the researchers Xing Chen, Zheng Guo, Gui-Mei Yang, Jie Li, Min-Qiang Li, Jin-Huai Liu, and Xing-Jiu Huang. The research paper is a comprehensive review of the work in the field of nanogap engineering as it relates to the application of electrical biosensing, covering strategies and design choices to enhance performance as well as to discuss optimizations and further development.

The planar nanogap refers to when both of the electrodes are faced with each other horizontally, as follows.

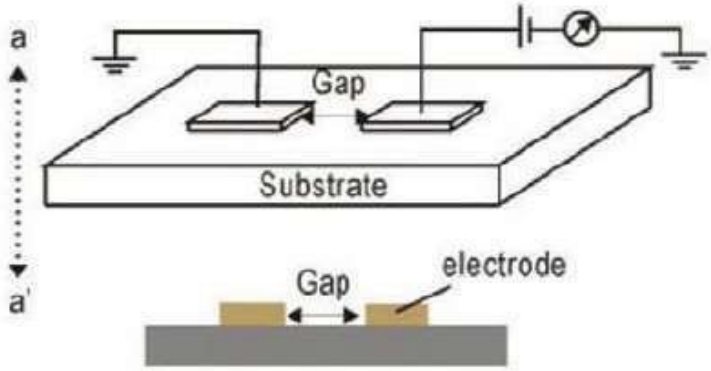

In the biosensing application, immobilized within the nanogap is a single stranded reference DNA, in which the capacitance is measured via a bias voltage, and the capacitance is predicated on the insulating properties of

the nanogap's material composition which are influenced by hybridization. The researchers note that immobilized oligonucleotides are tangled randomly, while, when they are hybridized to complementary DNA strands, a specific conformation is assumed. In addition, the parasitics emerge from the polysilicon electrodes, and more specifically the depletion effects in self-assembled monolayers. The researchers note the wide application of gold materials in nanogap biodevices, as there is advantageous bio- compatibility.

A challenge that is noted, within nanogap fabrication and engineering, is the examples of disadvantages and trade-offs in design, as well as common processing techniques not being suitable for high-throughput fabrication, such as electron beam lithography, mechanical break junction, and electromigration methods. It is noted that deposition methods can have issues in creating well-defined structures and patterns, and that thin film is a relatively complex process compared to what would be a more cost effective fabrication process. A device structure is noted for its great performance in analyzing individual DNA via a long nanofluidic channel which stretched the DNA into a linear chain, detecting via a pair of golden nanowires with 9nm gaps, as the nanogap detector, and it was able to measure electrical conductivity perpendicular to the DNA backbone. The researchers who conducted this study and application noted that for the detection resolution to improve for the nanogap's detection of single bases, there needs to be further optimizations on the nanogap dimensions, DNA mobility in the channel, and DNA translocation fluctuation times need to be improved.

Gold nanoparticles have also been used as ultrasensitive labels. In such an application, the immobilized probe DNA is within the narrow nanogap, where target DNA is co-hybridized to the electrode probe as well as a probe for signaling of the gold nanoparticles, in which these nanoparticles bridge the nanogap and assist in the detection of conductance changes of the targeted molecule. This configuration is shown in the following image.

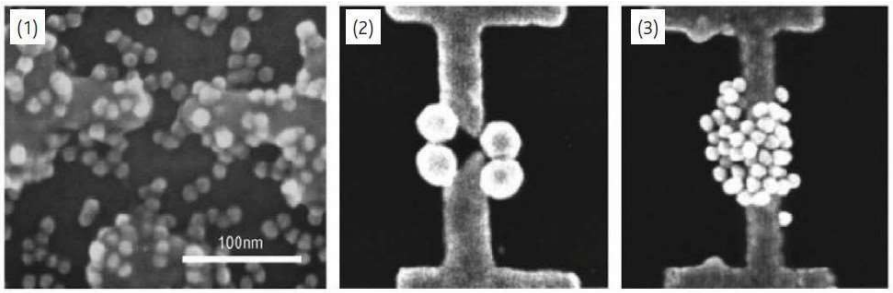

Gold colloidal particles are derived from the submonolayer gold colloidal particles deposited on the silicon dioxide substrate via the adhesion agent aminosilane, in which, afterwards, dithiol treatment is applied for added gold colloidal deposition, and these chains are bridged between the source and drain electrodes via electron beam lithography, seen in the above figure on the far left. This demonstrates the research and design of nanobridges constructed of nanoparticles for biomolecule detection. Even with this process, the nanoparticle synthesis is complex and takes a lot of time, in addition to the requirement of silver deposition to enhance the signal detection, obfuscating chip recycling and introducing further complexities as well as potentially lending itself to false positive detections. An enticing proposal to work around this issue is using dip-pen nanolithography and DNA-directed assembly. The dip-pen nanolithography processing technique allows molecule deposition on multitudes of surfaces which are coated with an atomic force microscope tip, functionalizing the nanoelectrode gap with the desired DNA sequences and complementary nanoparticles for selective hybridization. This process allows for multiple nanostructure assemblies onto a single chip.

The researchers note as well that nanometer size gaps with functionalized surfaces in the gap vicinities can be used to detect biological interactions, as the local surface functionalization is designed to be sensitive to the ligand/ receptor complex within the electrodes. The receptor has gold particle labeling smaller than the gap. In addition, different probing techniques are purported for having different capture properties. Immunoglobulin G, which is noted, can be captured and detected via protein proves and immobilized between the golden nanoelectrodes, and

these globulin proteins can even interact with secondary antibodies which are also labeled with golden nanoparticles, increasing conductance in the nanogap which can improve the capture and detection efficiency. However, there is more complex chemistry involved in using these labeled probes as well as additional expenses and other limiting factors.

Nanoparticles can also be used to enhance biosensing, without being used as labels, but instead to enhance the signal. One possible preliminary step is to use amplification techniques like PCR to amplify the DNA for the threshold to be met. However, not all biomolecules can utilize PCR or similar amplification techniques, hence the conductive nanoparticles being used to boost the signal. The benefits are large-scale integration, higher sensitivity, and easier read-out.

Gold nanoparticles can also be used to enhance layers, for example, the nanoparticles can reduce the distance of electron propagation between DNA molecules and act as hopping sites which amplify conductance of hybridized DNA strands, although single stranded DNA and gold nanoparticles exhibit low conductance. For the single stranded case, electrons will localize to the single stranded DNA without propagation, and the gold nanoparticles are limited to assisting the conductivity and signal amplification of the double stranded DNA

A promising technology for biosensing is the carbon nanotube nanogap device, with the major challenge being poorly-defined molecular-metal binding at the electrode. The work around for this is to use a SWCNT, in which the target molecule is immobilized in the gap between carbon nanotube electrodes. The target is detected via conductance changes in the electrodes, as a result.

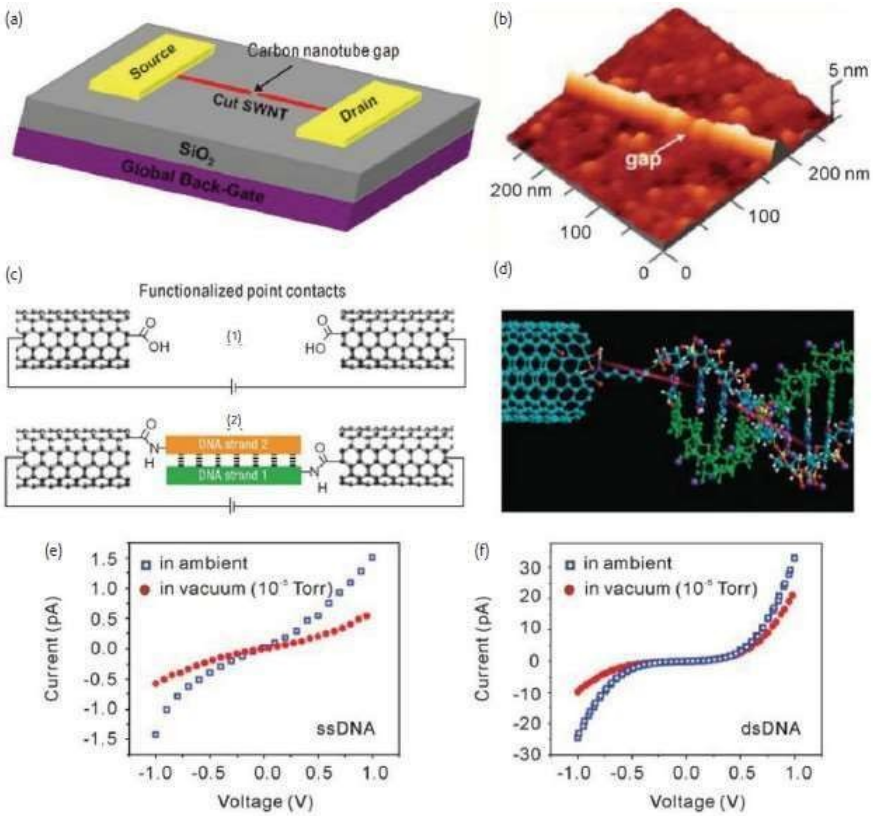

Carbon nanotube nanogap devices for biosensing. (a) A cut metallic SWCNT transistor connected by large metal leads as the S/D electrodes and the silicon wafer as the global back-gate[57]. (b) AFM image of the carbon nanotube nanogap[55]. (c) Illustration of sensing mechanism of carbon nanotube nanogap[57]. (1) Functionalized point contacts made through the precise cutting of a SWCNT with oxygen plasma. (2) Example of bridging by functionalization of both strands with amine functionality. (d) Molecular diagram highlighting the covalent bonding between an amine-terminated ssDNA and a carboxyl-functionalized SWCNT nanoelectrode via a $(-CH_2-)_6$ spacer. Charge transport takes place through the stacked base pairs in a helical duplex[63]. (e) and (f) Current flow at room temperature through single ssDNA and dsDNA molecules, respectively, in ambient and in vacuum conditions[63].

The benefit, with this design, is that with strong molecule-nanoelectrode coupling, the charge transport is not hindered by the coulomb blockade effect. Another benefit is that molecules attached via covalent bonding at the functionalized point contacts via amide linkages are useful in providing immunity from poor contact between molecules and the metal surface which occurs within thiol chemistry.

A nanotrench between the SWCNT electrodes will prevent the oxide surface from impacting the charge transport.

A vertical nanogap, consisting of two-terminal and three-terminal nanogaps, involves both electrodes vertically positioned in a perpendicular manner.

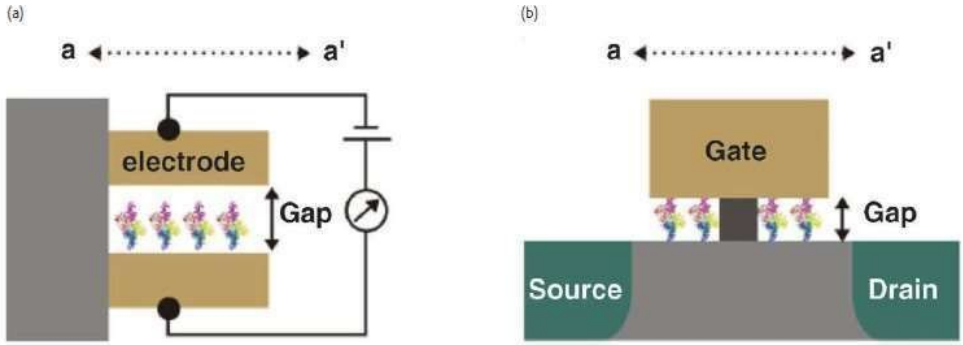

Vertical nanogap. Schematic of a FET device with a vertical nanogap for biomolecule sensing. a-a' direction of the dotted line shows the filled nanogap by biomolecules. (a) Two terminals. (b) Three terminals

For nanogap devices with two terminals, it is possible for the nanogap to act as a biomolecular junction due to its minimal size mitigating electrode polarization and being frequency immune in that regard. The bounded biomolecules purport dielectric changes which can then be sensed, in addition, ionic concentrations can influence the device characterization where it can be analytically modeled or investigated via the Poisson-Boltzmann equation. Another important factor is the aqueous environment within nanogaps and how it impacts biological processes such as protein folding, DNA hybridization, ligand-receptor complexes and other important biological mechanisms. There is research which studies this topic of how water and ice structures in nanogaps influence the biosensing characteristics. Oftentimes, the impedance will vary, due to frequency changes purported by the dielectric constant varying with biomolecules specific binding orientations within the nanogap. An advantage of impedance biosensors is that labeling is not required for detection, in addition to real-time monitoring.

As per nanogap devices with three terminals, the DMFET, which has been previously discussed in great detail, is a primary example with variations in design based on it. The researchers note that the device is novel due to its vertical configuration, and the advantage is that there is more design complexity compared to horizontal device configurations. Another

advantage is that standard CMOS processing techniques are employed, which may make them cheaper on average. Another advantage is that there are more degrees of freedom in nanogap engineering, material composition adjustments to suit different applications or optimize and observe performance changes, and the three-terminal nanogap devices have an easier time detecting dielectric properties of biomolecules with read-out circuitry.

The flexibility in the design means different calibrations which are suited for different applications and specific biosensing in mind with each targeted analyte. The researchers note a study in which a nanogap FET with a suspended chromium gate was developed. It had a bridge-like suspended gate, promoting free motion of biomolecules in and out of the cavity, and this application is suited as a proficient label-free biosensor, which is specifically targeted for the SBP-Ala protein, in the study.

To conclude the research article, a discussion of nanogap strategies was reported, evaluating the pros and cons to each method as well as limiting factors and promising future work within the respective fields. As a general principle, the detection of molecular binding events of very small concentrations of biomolecules, such as hybridization, as an example, is a major goal in the design of these biosensing devices. The literature was examined to evaluate the ongoing design and development of these nano- gap structures for this intended goal and purpose.

Final Remarks to the Chapter and the Thesis:

As a final remark to this chapter and this work, various studies have been evaluated to provide a general synopsis of the research and development undertaken in the design of double-gated dielectric modulated field effect transistors. In this investigative literature review, nanogap engineering techniques, biomechanical effects at the surface level and their respective effects on device performance based on orientation, charge profile, were examined, as well as within the nano-gap cavity structures in numerous examples, the impacts of biomolecular patterning and dielectric constants

as well as the general material composition effects on device performance were analytically modeled and studied. In addition, different topologies and variations were contrasted with one another to better understand the device operation, how characteristics were influenced by physical parameters such as device architecture, device geometries, materials properties, and the influence of the biomolecular charge, orientation, and mechanics on the transfer characteristics and other metrics observed.

A proposed design was modeled in Synopsys Sentaurus, discussing the advantages of the design, the physical characteristics and device operation, as well as the physics involved, and proposed changes in the model to optimize the behavior, documented in more specific detail within the first chapter.

As a final remark, I would like to thank you for reading this work. Please take care.

References/Bibliography of Literature Review Sources [IEEE Format]

---

[1] Rahul Das, Ankush Chattopadhyay, Manash Chanda, Chandan K. Sarkar, and Chayanika Bose. Analytical Modeling of Sensitivity Parameters Influenced by Practically Feasible Arrangement of Bio-Molecules in Dielectric Modulated FET Biosensor. Springer Nature.

[2] Monika Kumari, Niraj Kumar Singh, and Manodipan Sahoo. A detailed investigation of dielectric-modulated TMD FET based label-free biosensor via analytical modeling. Nature Scientific Reports.

[3] Ajay Singh, Mridula Gupta, Rakhi Narang, and Manoj Saxena. Investigation of Dielectric-Modulated Double-Gate Junctionless MOSFET for detection of biomolecules. Annual IEEE India Conference (INDICON).

[4] Dibyendu Chowdhury, Vishnu Prasad De, Bhargav Appasani, Navaneet Kumar Singh, Rajib Kar, Durbadal Mandal, Nicu Bizon, and Phatiphat Thounthong. A Novel Dielectric Modulated Gate-Stack Double-Gate Metal- Oxide-Semiconductor Field-Effect Transistor-Based Sensor for Detecting Biomolecules. MDPI. Special Issue Sensing and Measurement Technologies in Healthcare, Medicine, and Biosciences.

[5] Nirmali, Vijaya Kumar. Gate Engineering on the Analog Performance of DM-DG MOSFETs with High K Dielectrics. International Journal of Advanced Science and Technology volume. 25.

[6] Sayan Kanungo, Sanatan Chattopadhyay, Kunal Sinha, Partha Sarathi Gupta, and Hafizur Rahaman. A Device Simulation based Investigation on Dielectrically Modulated Fringing Field Effect Transistor for Biosensing Applications. IEEE Sensors Journal.

[7] Thomas Windbacher, V. Sverdlov, Siegfried Selberrherr, Clemens Heitzinger, Norbert Mauser, and Christian A. Ringhofer. Simulation of Field- Effect Biosensors (BioFETs). IEEE Xplore.

[8] Xing Chen, Zheng Guo, Gui-Mei Yang, Jie Li, Min-Qiang Li, Jin-Huai Liu, and Xing-Jiu Huang. Electrical nanogap devices for biosensing. Materials Today volume 13, Issue 11.